Repository of the Max Delbrück Center for Molecular Medicine (MDC) in the Helmholtz Association

Vascular signal transducer and activator of transcription-3 promotes angiogenesis and neuroplasticity long-term after stroke

Hoffmann, C.J., Harms, U., Rex, A., Szulzewsky, F., Wolf, S.A., Grittner, U., Laetig-Tuennemann, G., Sendtner, M., Kettenmann, H., Dirnagl, U., Endres, M., Harms, C.

Vascular Stat3 Promotes Angiogenesis and Neuroplasticity

Long-Term After Stroke

Running title: *Hoffmann et al.; Endothelial Stat3 and stroke*

Christian J. Hoffmann, MD[1,2]; Ulrike Harms, MD[1,2]; Andre Rex, MD[1]; Frank Szulzewsky, MSc[3];

Susanne A. Wolf, PhD[3]; Ulrike Grittner, PhD[1]; Gisela Lättig-Tünnemann, PhD[1];

Michael Sendtner, MD[4]; Helmut Kettenmann, PhD[3,5]; Ulrich Dirnagl, MD[1,5,6,7];

Matthias Endres, MD[1,2,5,6,7]; Christoph Harms, MD[1,2]

[1]Center for Stroke Research Berlin, Charité-Universitätsmedizin Berlin, Germany; [2]Dept of Neurology, Charité-Universitätsmedizin Berlin, Germany; [3]Max-Delbrück Center for Molecular Medicine, Berlin, Germany; [4]Institute of Clinical Neurobiology, University Hospital, University of Würzburg, Germany; [5]Cluster of Excellence NeuroCure, Charité-Universitätsmedizin Berlin, Germany; [6]German Center for Neurodegenerative Diseases (DZNE), Partner Site, Berlin, Germany; [7]German Center for Cardiovascular Diseases (DZHK), Partner Site, Berlin, Germany

Address for Correspondence:

Christoph Harms, MD

Center for Stroke Research

Charité-University Medicine Berlin

Robert-Koch Platz 4

D-10115 Berlin, Germany

Tel: +49 30 450 560 631

Fax: +49 30 450 560 930

E-mail: christoph.harms@charite.de

Abstract

Background—Post-stroke angiogenesis contributes to long-term recovery after stroke. Signal transducer and activator of transcription-3 (Stat3) is a key regulator for various inflammatory signals and angiogenesis. It was the aim of this study to determine its function in post stroke outcome.

Methods and Results—We generated a tamoxifen-inducible and endothelial-specific Stat3 knockout mouse model by crossbreeding Stat3$^{floxed/KO}$ and Tie2-Cre^{ERT2} mice. Cerebral ischemia was induced by 30 minutes of middle cerebral artery occlusion (MCAo). We demonstrated that endothelial Stat3 ablation did not alter lesion size 2 days after ischemia but did worsen functional outcome at 14 days and increase lesion size at 28 days. At this late time point vascular Stat3 expression and phosphorylation were still increased in wildtype mice. Gene array analysis of a CD31-enriched cell population of the neurovascular niche showed that endothelial Stat3 ablation led to a shift toward an anti-angiogenic and axon growth-inhibiting micro-milieu after stroke, with an increased expression of Adamts9. Remodeling and glycosylation of the extracellular matrix (ECM) as well as microglia proliferation were increased while angiogenesis was reduced.

Conclusions—Endothelial Stat3 regulates angiogenesis, axon growth and ECM-remodeling and is essential for long-term recovery after stroke. It might serve as a potent target for stroke treatment after the acute phase by fostering angiogenesis and neuroregeneration.

Key words: cerebral ischemia, angiogenesis, inflammation, gene microarray, endothelial cell

Introduction

Long-term recovery after brain ischemia is linked to angiogenesis. How newly formed vessels can improve functional outcome is unclear. Angiogenesis restores oxygen and nutrient supply to the affected brain tissue, but post-stroke angiogenesis starts too late to interact with ischemic cell death cascades. The newly formed vessels seem to be more relevant for regenerative mechanisms such as neurogenesis, axonal growth and synaptic plasticity.[1] Angiogenesis and neurogenesis are intricately linked.[2] Axonal growth cones and endothelial tip cells of sprouting vessels share many features and respond to the same signaling pathways.[3] Angiogenic vessels provide neurotrophic support to newly generated neurons and facilitate synaptogenesis.[4]

Treatments are needed that foster regeneration at later time points. Strategies focusing on angiogenesis are ambivalent. Most angiogenic factors like vascular endothelial growth factor (Vegf) may increase vascular permeability and thus increase edema formation. In addition, angiogenesis is strongly related to inflammatory pathways. For instance, Vegf as well as Interleukin 6 (Il6) converge on the Signal Transducer and Activator of Transcription-3 (Stat3) signaling pathway; on the other hand activation of Stat3 by Il6 increases Vegf production.[5] In endothelial cells Stat3 activation promotes angiogenesis by regulating endothelial cell migration and proliferation[6] and is involved in vascular diseases such as pulmonary hypertension.[7]

Stat3 shows neuroprotective properties in the acute phase of stroke, inhibiting apoptosis and scavenging reactive oxygen species (ROS) in neurons, thereby reducing infarct size.[8,9,10,11,12,13] It might however induce detrimental effects in the sub-acute phase after stroke. It has been shown that Stat3 is mainly expressed and activated in microglia and macrophages 24-72 hours after cerebral ischemia.[14] Blocking Stat3 phosphorylation within the first 72 hours reduced lesion size; this effect is mediated by an inactivation of Stat3 in microglia and macrophages.

3

Following brain ischemia, endothelial cells seem to express and phosphorylate Stat3 later than neurons and microglia, beginning at 48 hours and continuing for at least 7 days.[8] This is the time window in which expression and phosphorylation of Stat3 by endothelial cells reach their highest levels compared to those of other cell types.[8] This delayed activation of the angiogenic Stat3 pathway in endothelial cells after cerebral ischemia may indicate an important function of endothelial Stat3 in regenerative mechanisms. We previously demonstrated that lack of Il6 increased lesion size and worsened functional outcome 28 days after ischemia. The underlying mechanism seemed to be a reduction of angiogenesis.[15]

It was therefore the aim of this study to search for the specific role of endothelial Stat3 in the pathophysiology of cerebral ischemia and in particular its effects on post-stroke angiogenesis and long-term outcome. To obtain a knockout of Stat3 which is restricted to endothelial cells *in vivo,* we used an inducible endothelial-specific Stat3 knockout mouse model by crossbreeding Stat3$^{floxed/KO}$ mice[16] with Tie2-Cre^{ERT2} mice[17] (endothelial-Tie2-Cre^{ERT2};Stat3$^{floxed/KO}$). Tie2-Cre^{ERT2} littermates treated with tamoxifen served as controls. Cerebral ischemia was induced by filamentous occlusion of the A. cerebri media for 30 min (MCAo). This study shows for the first time that endothelial Stat3 activation is necessary for post-stroke angiogenesis, alters long-term lesion size and plays a beneficial role in functional improvement after stroke. Endothelial loss of Stat3 leads to an anti-angiogenic and axon growth inhibiting micro-milieu within the neurovascular niche with induced Adamts9 expression and consequently an altered remodeling of the extracellular matrix.

Methods

A detailed method section is provided in the Online Data Supplements.

Animals and treatments

All animal experiments were approved by the local governmental authorities (Landesamt für Gesundheit und Soziales, G0354/11). Stat3[floxed/KO] mice[16] were crossbred with Tie2-Cre[ERT2] mice[17]. Endothelial-specific knockout of Stat3 was induced by a 5 day i.p. application of tamoxifen (1 mg/d) 7 days prior to surgery. Tie2-Cre[ERT2] littermates were treated with tamoxifen and served as a control group. In a total of 3 animals – two wildtype mice and 1 knockout animal – no lesions developed. These 3 animals were excluded from the study.

Model of middle cerebral artery occlusion (MCAo)

Filamentous middle cerebral artery occlusion of the left side was performed for 30 minutes with indicated reperfusion time points according to the published standard operating procedure in our laboratory[18] in the DIN9001-certified laboratories of the Department of Experimental Neurology at the Charité.

Real-time RT-PCR

RNA from slices of ischemic and contralateral hemispheres was extracted using Trizol (Invitrogen). 1 µg of RNA was transcribed with MLV-reverse transcriptase (Promega). Real-time PCR was performed with intron spanning primers for tyrosine 3-monooxygenase/tryptophan 5-monooxygenase activation protein (Ywhaz) and succinate dehydrogenase complex, subunit A, flavoprotein (Sdha) as internal controls[19], and primers for Stat3 using Sybr green (Qiagen). Foldamount of mRNA compared to mean of internal controls was calculated using the equation: $2^{-(Ct(gene\ of\ interest)-Ct(internal\ control))}$

Histology and immunofluorescence

Mice were placed under deep anesthesia, cardially perfused with NaCl-solution, and decapitated. The brains were snap frozen in -40 °C isopentane for cryostat sectioning 2 and 28 days after

MCAo. 20 µm cryosections were fixed with aceton/methanol and stained for caveolin-1, pStat3 (Tyr705), BrdU, NeuN, isolectin-B4, Adamts9. Cytospins after CD31 MACS were stained for caveolin-1. Orthogonal projections of vascular networks in the peri-infarct region were stained with isolectin-B4 (see online supplements for details).

Lesion volume determination and functional outcome

We quantified cerebral lesion volume with ImageJ analysis software (NIH, USA) on 20 µm NeuN-DAB-stained cryostat sections and calculated volume by summing up the infarct sizes of each section as previously described[18] or by T2-weighted MRI imaging. Functional outcome was determined with behavioral tests (Rotarod test and the extended neuroscore). To determine lesion size we used a total of 16 endothelial-Tie2-Cre^{ERT2};Stat3$^{floxed/KO}$ and 23 Tie2-Cre^{ERT2} littermates. All underwent MRI at 2 days after ischemia. A subset of 9 endothelial-Tie2-Cre^{ERT2};Stat3$^{floxed/KO}$ and 12 Tie2-Cre^{ERT2} littermates was killed at 2 days after ischemia and a subset of 7 endothelial-Tie2-Cre^{ERT2};Stat3$^{floxed/KO}$ and 11 Tie2-Cre^{ERT2} littermates at 28 days for histological lesion size determination. For behavioral tests 12 endothelial-Tie2-Cre^{ERT2};Stat3$^{floxed/KO}$ and 12 Tie2-Cre^{ERT2} littermates were used.

ELISA

ELISA assays for determining Vegf (R&D systems) and Il6 (Invitrogen) levels were performed according to manufacturer's instructions.

Isolation of CD31-enriched cells

Mice were killed 4 days after cerebral ischemia. The ipsi- and contralateral hemispheres were divided and processed separately. Hemispheres from 7 animals were pooled. The tissue was dissociated using the Papain Neural Tissue Dissociation Kit (Miltenyi Biotec). Myelin was removed following a protocol published elsewhere.[20] Cells were labeled with anti-CD31

microbeads™ (Miltenyi Biotec). We performed MACS isolation according to the manufacturer's instructions. Total RNA from MACS was isolated using the RNeasy Plus Mini Kit (Qiagen). A total of 21 endothelial-Tie2-Cre^{ERT2};Stat3$^{floxed/KO}$ and 21 Tie2-Cre^{ERT2} littermates was used and divided to 3 groups each before isolation.

GeneChip microarray assay

Sample preparation for microarray hybridization was carried out as described in the Ambion WT Expression Kit Protocol (Life Technologies) and the Affymetrix WT Terminal Labeling and Hybridization User Manual (Affymetrix, Inc.).

Sample processing was performed at an Affymetrix Service Provider and Core Facility, "KFB - Center of Excellence for Fluorescent Bioanalytics" (Regensburg, Germany; www.kfb-regensburg.de).

Microarray data analysis

Summarized probe set signals were calculated by using the RMA[21] algorithm with the Affymetrix GeneChip Expression Console Software. Probe sets with a fold change above 2.0 fold and a Student's t test P value lower than 0.05 were considered as significantly regulated with n=3 independent experiments.

FACS

Co-expression of anti-mouse CD11b-APC and CD45-efluor™450 are shown in density plots. CD11b$^+$CD45^{hi} cells infiltrate monocytes/macrophages while CD11b$^+$CD45^{low} are the intrinsic microglial population.

Statistical analysis

All data are presented as scatter dot plots with mean ± standard deviation. Detailed description of statistical analysis is provided in the figure legends and in the Online Data Supplements.

Results

Conditional ablation of endothelial Stat3

An endothelial-specific conditional knockout mouse for Stat3 was generated by crossbreeding endothelial specific Cre[ERT2] mice (Tie2-Cre[ERT2] mice) with Stat3[floxed/KO] mice which have the exon 22 of Stat3 flanked by LoxP sites. A phosphorylation of the tyrosine residue at position 705 in the protein domain encoded by the exon 22 is indispensable for activation of Stat3. We used the Tie2-Cre[ERT2] mouse generated by Forde et al. (MGI:2450312)[17], which showed highly specific endothelial expression with negligible expression in hematopoietic cells. To test efficacy and specificity of endothelial-Tie2-Cre[ERT2];Stat3[floxed/KO] after tamoxifen administration we performed immunofluorescence co-staining of pStat3(Y705) and caveolin-1. Phosphorylation of Stat3 was induced by ischemia. We observed a significant decrease of phosphorylated Stat3$^+$/caveolin-1$^+$ endothelial cells of Tie2-Cre[ERT2];Stat3[floxed/KO] mice compared to their Tie2-Cre[ERT2] littermates (**Figure 1A and B**). As expected, we observed no reduction of phosphorylated Stat3 in caveolin-1 negative or non-endothelial cells in endothelial-Tie2-Cre[ERT2];Stat3[floxed/KO] mice (**Figure 1A and C**). However, we did observe pStat3$^+$/caveolin-1$^+$ cells in endothelial Tie2-Cre[ERT2];Stat3[floxed/KO] mice with tamoxifen treatment and ischemia. In endothelial cells the loss of pStat3(Y705) was still evident at 28 days.

Increased gene expression and Stat3 phosphorylation 28 days after ischemia

We determined the expression of Stat3 mRNA after a 30 minute occlusion of the left middle cerebral artery (MCAo) and differing reperfusion times up to 28 days after ischemia. In the ischemic hemisphere there was a strong increase in Stat3 expression. The mRNA level was highest 2 days after reperfusion (4-fold induction) and then declined again at 3 days after reperfusion, but levels were still elevated at 28 days (**Figure 1D**). No induction took place at any

time in the non-ischemic hemisphere. The amount of activated Stat3 in endothelial cells was determined by immunofluorescence co-stainings for pStat3 and caveolin-1 at 2 days and 28 days after cerebral ischemia. In endothelial cells of the peri-infarct area, Stat3 was still being phosphorylated at 28 days. Furthermore, at this time point significantly more endothelial cells were immunoreactive for pStat3 than had been the case 2 days after ischemia (**Figure 1E**).

Conditional ablation of endothelial Stat3 causes worse long-term stroke outcome

A control group of Endothelial-Tie2-Cre^{ERT2};Stat3$^{floxed/KO}$ and Tie2-Cre^{ERT2} littermates received tamoxifen for five consecutive days and was subjected 2 days later to 30 min MCAo (**Figure 2A**). In MRI imaging 2 days after ischemia no difference was detected between the genotypes (**Figure 2B and C**). A subset of both genotypes (n=12 Tie2-Cre^{ERT2} littermates and n=9 Tie2-Cre^{ERT2};Stat3$^{floxed/KO}$ mice) was killed for histological evaluation of lesion size at 2 days after ischemia. NeuN-immunohistochemistry and quantification of the lesion size consistently failed to reveal any difference in the degree of neuronal loss between endothelial-Tie2-Cre^{ERT2};Stat3$^{floxed/KO}$ and Tie2-Cre^{ERT2} littermates (**Figure 2D and E**). However, at 28 days after ischemia we observed that genomic ablation of Stat3 had led to lesion sizes which were larger than those in Tie2-Cre^{ERT2} littermates (**Figure 3A and B**). At 14 days after 30 min MCAo functional outcome as tested by behavioral analysis was worse: In the Rotarod test the 'time-to-drop' was significantly lower (**Figure 3C**) and the extended neuroscore in endothelial-Tie2-Cre^{ERT2};Stat3$^{floxed/KO}$ mice was lower (**Figure 3D**). Taken together, ablation of endothelial Stat3 had no effect on short-term post stroke outcome. In fact, at 14 days post stroke the functional outcome was worse and at 28 days after stroke lesion volume was greater.

Endothelial Stat3 promotes angiogenesis after cerebral ischemia

Next, we analyzed angiogenesis after cerebral ischemia and endothelial Stat3 ablation. Vessel

density was determined by measuring the caveolin-1 positive area (see methods for details). We observed at 28 days after reperfusion that endothelial ablation of Stat3 had reduced vessel density (**Figure 4A and C**). The number of caveolin-1 / BrdU double-positive cells was significantly reduced by 60% ($p < 0.005$) (**Figure 4B and D**) indicating a reduced proliferation of endothelial cells. Vessel density in peri-infarct striatal regions was reduced as visualized after 3D rendering of confocal Z-stacks (**Figure 4E and F**, **Supplemental movie**). Il6 induces the expression of Vegf by activating the Stat3 signaling pathway. At 2 days and 28 days after MCAo we measured the serum levels of Il6 and Vegf using ELISA. There was no difference between the two genotypes, either at 2 days or 28 days, either for Il6 or Vegf (**Supplemental Figure 1A and B**, Supplemental Material).

Endothelial Stat3 ablation is followed by increased percentage of CD11b$^+$/CD45^{low} cells and of CD11b$^+$/CD45^{high} cells

With FACS analysis at 4 days after MCAo we determined the percentage of CD11b$^+$/CD45^{low} and CD11b$^+$/CD45^{high} cells in the total cell population. It is generally assumed that CD11b$^+$/CD45^{low} are microglial cells and that CD11b$^+$/CD45^{high} cells represent invading myeloide cells. We found an increase of CD11b$^+$/CD45^{low} cells in the ischemic hemisphere compared to the contralateral hemisphere, and this increase was significantly higher after endothelial Stat3 ablation (**Figure 4G and H**). In Tie2-Cre^{ERT2} littermates we found a slight trend towards increased invasion of myeloide cells in the ischemic hemisphere compared to the contralateral side, whereas a significant increase of invading myeloide cells was evident in endothelial-Tie2-Cre^{ERT2};Stat3$^{floxed/KO}$. However, the number of myeloide cells in the ischemic hemisphere did not differ significantly between endothelial-Tie2-Cre^{ERT2};Stat3$^{floxed/KO}$ and Tie2-Cre^{ERT2} littermates.

Endothelial Stat3 ablation results in an anti-angiogenic, axon growth-inhibiting and extracellular matrix (ECM)-degrading micro-milieu

We analyzed the transcriptional profile of CD31-enriched cells at 4 days after cerebral ischemia and endothelial Stat3 ablation. Our isolation and enrichment method maintains the interaction between endothelial cells and adjacent cells. We determined the cellular composition of the isolated cells by immunostaining cytospins after CD31-MACS and found endothelial cells to be the dominant fraction (**Figure 5A**). We found marker genes for endothelial cells, neurons, astrocytes and oligodendrocytes to be present in the isolated RNA (**Figure 5B**). In summary, the isolated cell population reflects the cellular composition of the neurovascular niche.

The expression of 255 genes differed significantly – by more than 2-fold – between the genotypes (**Supplemental Table 1**). Gene arrays were performed from three independent experiments with 7 animals per experiment and genotype (in total 21 Tie2-Cre^{ERT2};Stat3$^{floxed/KO}$ and 21 Tie2-Cre^{ERT2} littermates). Overall, we found a complex network response with an increase of anti-angiogenic factors and a decrease of angiogenic factors after endothelial Stat3 ablation (**Figure 5C** and **Table 1**). Moreover, we observed an increase of factors that inhibit axonal growth and a decrease of factors that promote axonal growth (**Figure 5D** and **Table 2**). We also identified a decreased expression of several components of the ECM and an induction of ECM degrading enzymes. Interestingly, Adamts9, a potent anti-angiogenic and ECM-degrading enzyme, is strongly induced after endothelial Stat3 ablation. In the rat it is reported to be expressed exclusively in neurons and astrocytes directly after cerebral ischemia.[22] In immune staining we found Adamts9 to be expressed mainly in endothelial cells of the peri-ischemic area at 4 days after ischemia (**Figure 6A**). Additionally, we found a slight but significant increase of ROS-producing genes like iNOS and NOX4 and induced expression of CD14 (**Table 1**,

supplements). These changes point to an increased inflammatory activation after endothelial Stat3 ablation.

In summary, endothelial Stat3 ablation leads to a shift of the transcriptional profile within the neurovascular niche towards an anti-angiogenic and axon growth inhibiting micro-milieu. Moreover, we found a shift towards an ECM degrading micro-milieu.

Endothelial Stat3 ablation changes the glycosylation pattern of the ECM after cerebral ischemia

The composition of the ECM changes after cerebral ischemia.[23] Prominently, the expression of proteogylcans is increased. This type of ECM composition hinders growing axons from entering the lesion volume and thereby impairs axonal plasticity and functional recovery. The axon growth inhibiting properties of the proteoglycans are conditioned by the glycosylation pattern of the glycosaminoglycan side chains.[23] Isolectin-B4 is a lectin derived from *Griffonia simplicifolia* that binds terminal α-D-galactosyl residues which are present mainly on the surface of endothelial and monocytic cells. It has been shown that isolectin-B4 binds the proteoglycan versican.[24] We stained the brains with isolectin-B4 at 28 days after cerebral ischemia to identify functional changes in ECM in the genotypes. With isolectin-B4 we found an increased staining of the ECM in the ischemic area (**Figure 6 B**). Moreover, the volume of the isolectin-B4 positive ECM-area increased after endothelial Stat3 ablation (**Figure 6B and C**).

Discussion

The major finding of this study is that activation of endothelial Stat3 is crucial for long-term outcome after stroke. We generated an endothelial-specific and inducible knockout mouse model by crossbreeding mice (Tie2-Cre[ERT2];Stat3[floxed/KO]) to analyze the function of endothelial Stat3 in

stroke. Endothelial Stat3 ablation caused increased lesion size in the long-term after stroke, but not in the short-term. Angiogenesis was reduced while the percentage of microglia increased, indicating microglia proliferation. The expression profile within the neurovascular niche was changed to an anti-angiogenic, axon growth inhibiting micro-milieu with ECM degradation. Most prominently, expression of the anti-angiogenic and proteoglycan-cleaving Adamts9 was induced after endothelial Stat3 ablation and cerebral ischemia. We found Adamts9 to be expressed mainly in endothelial cells in the peri-ischemic area. Moreover, after endothelial Stat3 ablation we found altered glycosylation patterns of the ECM. In the end, functional outcome was worse after endothelial Stat3 ablation and cerebral ischemia.

Short-term analysis of lesion volumes 2 days after reperfusion revealed no differences between the genotypes, either in MRI or in histology, after 30 min MCAo (**Figure 2A-D**). This confirms previous data on the kinetics of Stat3 phosphorylation: Stat3 is highly induced and activated in neurons in the ischemic core and peri-infarct region within 8 hours after stroke.[8] Stat3 exerts its anti-apoptotic effects in neurons.[11, 25, 26] Stat3 phosphorylation in contrast does not start in endothelial cells before 48 hours after ischemia.[8] An endothelial-specific knockout of Stat3 should therefore not impact on the acute outcome after stroke. Our results thus fit nicely together with the known kinetics of endothelial Stat3. We compared genotype lesion sizes at 28 days after ischemia and detected yet upregulated and phosphorylated Stat3 in endothelial cells (**Figure 1D and E**). Endothelial Stat3 ablation increased the lesion volume at this later time point (**Figure 3A and B**).

At 28 days after ischemia vessel density (**Figure 4A and C**) and endothelial cell proliferation (**Figure 4B and D**) were reduced after endothelial Stat3 ablation. After cerebral ischemia Stat3 is activated by several inflammatory factors such as Il6, Lif or Cntf.[27-29]

Activation of Stat3 by Il6 is followed by increased angiogenesis which is in part mediated by transcriptional induction of Vegf.[30] This led us to seek differences in Il6 and Vegf serum levels after endothelial knockout of Stat3. Contrary to our expectations, however, endothelial ablation of Stat3 had no impact on systemic Il6 or Vegf levels (**Figure 1A and B**, supplements). Endothelial Stat3 is apparently not involved in elevated Il6 serum levels after cerebral ischemia, and the induction of angiogenesis after stroke by Stat3 activation is independent of Vegf.

We established a method to isolate endothelial cells and adjacent cells of the neurovascular niche after endothelial Stat3 ablation and cerebral ischemia and we analyzed the transcriptional profile of this cell population by gene array analysis. Capillary endothelial cells are embedded in a firm basal membrane consisting mainly of collagens. The triple helix structure of collagens can be destroyed by collagenase digestion but is resistant to cleavage by trypsin, pepsin or papain.[31] Therefore we digested the brain matrix with papain to maintain the interaction between the basal membrane of the vasculature and the adherent cells of the neurovascular niche. Endothelial cells and all adherent cells were isolated by CD31-MACS. We chose a time point 4 days after ischemia, when angiogenesis and axonal growth are still going on but mechanisms of the acute phase after ischemia have already ceased.

In the CD31-enriched population 4 days after cerebral ischemia, we identified 255 genes which showed differing expression levels between genotypes (**Supplemental Table 1**). Overall endothelial Stat3 ablation led to an anti-angiogenic and axon growth inhibiting micro-milieu (**Figure 5A and B**). Interestingly, endothelial Tie2-Cre[ERT2];Stat3[floxed/KO] mice showed higher expression of apelin, apelin receptor and placental growth factor – all potent angiogenic factors – than did their Tie2-CreERT2 littermates. This might indicate a compensatory activation of alternative angiogenic pathways which after activation, however, did not change angiogenesis. It

is known that after ischemia, the outgrowing vessels support neuroblast migration in a scaffold-like manner, directing migration to the damaged areas.[2] The reduction of angiogenesis after endothelial Stat3 ablation precludes this process and might thus contribute to impaired neuroplasticity.

Most prominent was an increased expression of Adamts9 with strong anti-angiogenic activity.[32] It is reported that Adamts9 in the rat is mainly expressed in neurons 24 hours after cerebral ischemia.[22] We found its expression mainly in endothelial cells in the peri-ischemic tissue 4 days after ischemia. Adamts proteases are classified in three sub-families based on their preference for cleaving specific ECM components.[33] Adamts9 belongs to the proteoglycanases and degrades chondroitin sulfate proteoglycans (CSPGs). CSPGs are major components of the ECM and are characterized by a core protein with at least one covalently bound glycosaminoglycan side chain and a variable number of N- and O-linked oligosaccharides.

After cerebral ischemia the composition of the ECM is changed to a more 'juvenile matrix type'.[34] Therefore the ECM first has to be degraded. In proteoglycans this is performed predominantly by Adamts proteases. Finally the expression of all proteoglycans is much higher after ischemia, and they contribute to a large extent to the development of the ECM component in the lesion volume. The chronic lesion volume on the one hand improves the physical stability of the ischemic area, on the other hand it strongly impairs neuroplasticity.[23] Thus digestion of proteoglycans by Adamts proteases is thought to have beneficial effects.[33] Endothelial Stat3 ablation led to an intense upregulation of Adamts9 which quite specifically cleaves the long variants of the proteoglycans – aggrecan and versican – but not the short proteoglycan brevican. However, the expression of the short proteoglycans neurocan and brevican was reduced, as was the expression of tenascinR. Also reduced was the expression of phosphacan and its cellular

binding partners Ncam, Nrcam and contactin2.

In general, the expression pattern of the matrix within the neurovascular niche was shifted towards the 'juvenile matrix type' with a looser mesh-size and thus axon growth-promoting ECM-environment, with less inter-cellular ECM binding after endothelial Stat3 ablation. Nonetheless, the expression of other axon growth inhibiting genes and the suppression of growth promoting genes seemed to outweigh this effect after endothelial Stat3 ablation. Adamts9 expression was not able to reduce chronic lesion size or improve functional outcome. Furthermore, in isolectin-B4 staining we found an increase of α-D-galactosyl residues in the chronically damaged tissue. The axon growth inhibiting activity of proteoglycans is partly mediated by their glycosylation patterns. Endothelial Stat3 might be highly relevant for regulation of the glycosylation pattern of the ECM in the chronic lesion and might thereby influence axon growth and neuroplasticity.

Beyond that, we found a slightly increased invasion of monocytes 4 days after cerebral ischemia and endothelial Stat3 ablation. Proliferation of microglia was increased. The expression of ROS-building genes such as iNOS and NOX4 as well as CD14 was higher, which might contribute to delayed neuronal cell death and increased lesion size in the long-term after ischemia.

As a consequence, treatment strategies that focus on Stat3 signalling of endothelial cells offer the following three advantages: 1) accessibility for intravenous treatment, 2) treatment options in the acute phase of stroke beyond the narrow time window for thrombolysis, 3) pleiotropic neuroregenerative action with widespread consequences for brain plasticity through changes in the micro-environment. Although this study provides substantial insight into the consequences of endothelial Stat3 signalling on long-term outcome after cerebral ischemia,

further studies need to address the beneficial effects of endothelial-specific Stat3 signalling as a

treatment option. We suggest using drugs that do not pass the blood brain barrier in order to

achieve an endothelial-specific stimulation of Stat3 and avoid activation of microglial Stat3,

which might have detrimental consequences.

Conflict of Interest Disclosures: None.

References:

1. Beck H, Plate KH. Angiogenesis after cerebral ischemia. *Acta Neuropathologica*. 2009;117:481-496.

2. Young CC, Brooks KJ, Buchan AM, Szele FG. Cellular and molecular determinants of stroke-induced changes in subventricular zone cell migration. *Antioxid Redox Signal*. 2011;14:1877-1888.

3. Adams RH, Eichmann A. Axon guidance molecules in vascular patterning. *Cold Spring Harb Perspect Biol*. 2010;2:a001875.

4. Ohab JJ, Fleming S, Blesch A, Carmichael ST. A neurovascular niche for neurogenesis after stroke. *Journal Neurosci*. 2006;26:13007-13016.

5. Funamoto M, Fujio Y, Kunisada K, Negoro S, Tone E, Osugi T, Hirota H, Izumi M, Yoshizaki K, Walsh K, Kishimoto T, Yamauchi-Takihara K. Signal transducer and activator of transcription 3 is required for glycoprotein 130-mediated induction of vascular endothelial growth factor in cardiac myocytes. *J Biol Chem*. 2000;275:10561-10566.

6. Yahata Y, Shirakata Y, Tokumaru S, Yamasaki K, Sayama K, Hanakawa Y, Detmar M, Hashimoto K. Nuclear translocation of phosphorylated STAT3 is essential for vascular

endothelial growth factor-induced human dermal microvascular endothelial cell migration and tube formation. *J Biol Chem*. 2003;278:40026-40031.

7. Paulin R, Meloche J, Bonnet S. STAT3 signaling in pulmonary arterial hypertension. *Jak-Stat*. 2012;1:223-233.

8. Suzuki S, Tanaka K, Nogawa S, Dembo T, Kosakai A, Fukuuchi Y. Phosphorylation of signal transducer and activator of transcription-3 (Stat3) after focal cerebral ischemia in rats. *Exp Neurol*. 2001;170:63-71.

9. Loddick SA, Turnbull AV, Rothwell NJ. Cerebral interleukin-6 is neuroprotective during permanent focal cerebral ischemia in the rat. *J Cereb Blood Flow Metab*. 1998;18:176-179.

10. Battle TE, Frank DA. The role of STATs in apoptosis. *Curr Mol Med*. 2002;2:381-392.

11. Jung JE, Kim GS, Narasimhan P, Song YS, Chan PH. Regulation of Mn-superoxide dismutase activity and neuroprotection by STAT3 in mice after cerebral ischemia. *J Neurosci*. 2009;29:7003-7014.

12. Yamashita T, Sawamoto K, Suzuki S, Suzuki N, Adachi K, Kawase T, Mihara M, Ohsugi Y, Abe K, Okano H. Blockade of interleukin-6 signaling aggravates ischemic cerebral damage in mice: possible involvement of Stat3 activation in the protection of neurons. *J Neurochem*. 2005;94:459-468.

13. Dziennis S, Jia T, Ronnekleiv OK, Hurn PD, Alkayed NJ. Role of signal transducer and activator of transcription-3 in estradiol-mediated neuroprotection. *J Neurosci*. 2007;27:7268-7274.

14. Satriotomo I, Bowen KK, Vemuganti R. JAK2 and STAT3 activation contributes to neuronal damage following transient focal cerebral ischemia. *J Neurochem*. 2006;98:1353-1368.

15. Gertz K, Kronenberg G, Kalin RE, Baldinger T, Werner C, Balkaya M, Eom GD, Hellmann-Regen J, Krober J, Miller KR, Lindauer U, Laufs U, Dirnagl U, Heppner FL, Endres M. Essential role of interleukin-6 in post-stroke angiogenesis. *Brain*. 2012;135:1964-1980.

16. Takeda K, Kaisho T, Yoshida N, Takeda J, Kishimoto T, Akira S. Stat3 activation is responsible for IL-6-dependent T cell proliferation through preventing apoptosis: generation and characterization of T cell-specific Stat3-deficient mice. *J Immunol*. 1998;161:4652-4660.

17. Forde A, Constien R, Grone HJ, Hammerling G, Arnold B. Temporal Cre-mediated recombination exclusively in endothelial cells using Tie2 regulatory elements. *Genesis*. 2002;33:191-197.

18. Endres M, Gertz K, Lindauer U, Katchanov J, Schultze J, Schrock H, Nickenig G, Kuschinsky W, Dirnagl U, Laufs U. Mechanisms of stroke protection by physical activity. *Ann Neurol*. 2003;54:582-590.

19. Gubern C, Hurtado O, Rodriguez R, Morales JR, Romera VG, Moro MA, Lizasoain I, Serena J, Mallolas J. Validation of housekeeping genes for quantitative real-time PCR in in-vivo and in-vitro models of cerebral ischaemia. *BMC Mol Biol*. 2009;10:57.

20. Olah M, Amor S, Brouwer N, Vinet J, Eggen B, Biber K, Boddeke HW. Identification of a microglia phenotype supportive of remyelination. *Glia*. 2012;60:306-321.

21. Irizarry RA, Hobbs B, Collin F, Beazer-Barclay YD, Antonellis KJ, Scherf U, Speed TP. Exploration, normalization, and summaries of high density oligonucleotide array probe level data. *Biostatistics*. 2003;4:249-264.

22. Reid MJ, Cross AK, Haddock G, Allan SM, Stock CJ, Woodroofe MN, Buttle DJ, Bunning RA. ADAMTS-9 expression is up-regulated following transient middle cerebral artery occlusion (tMCAo) in the rat. *Neurosci Lett*. 2009;452:252-257.

23. Yiu G, He Z. Glial inhibition of CNS axon regeneration. *Nat Rev Neurosci*. 2006;7:617-627.

24. Bogen O, Dreger M, Gillen C, Schroder W, Hucho F. Identification of versican as an isolectin B4-binding glycoprotein from mammalian spinal cord tissue. *FEBS J*. 2005;272:1090-1102.

25. Jung JE, Kim GS, Chan PH. Neuroprotection by interleukin-6 is mediated by signal transducer and activator of transcription 3 and antioxidative signaling in ischemic stroke. *Stroke*. 2011;42:3574-3579.

26. Kinouchi T, Kitazato KT, Shimada K, Yagi K, Tada Y, Matsushita N, Sumiyoshi M, Satomi J, Kageji T, Nagahiro S. Activation of signal transducer and activator of transcription-3 by a peroxisome proliferator-activated receptor gamma agonist contributes to neuroprotection in the peri-infarct region after ischemia in oophorectomized rats. *Stroke*. 2011;43:478-483.

27. Ali C, Nicole O, Docagne F, Lesne S, MacKenzie ET, Nouvelot A, Buisson A and Vivien D. Ischemia-induced interleukin-6 as a potential endogenous neuroprotective cytokine against NMDA receptor-mediated excitotoxicity in the brain. *J Cereb Blood Flow Metab*. 2000;20:956-966.

28. Lin TN, Wang PY, Chi SI, Kuo JS. Differential regulation of ciliary neurotrophic factor (CNTF) and CNTF receptor alpha (CNTFR alpha) expression following focal cerebral ischemia. *Brain Res Mol Brain Res*. 1998;55:71-80.

29. Suzuki S, Tanaka K, Nogawa S, Ito D, Dembo T, Kosakai A, Fukuuchi Y. Immunohistochemical detection of leukemia inhibitory factor after focal cerebral ischemia in rats. *J Cereb Blood Flow Metab*. 2000;20:661-668.

30. Chen Z, Han ZC. STAT3: a critical transcription activator in angiogenesis. *Med Res Rev*. 2008;28:185-200.

31. Kadler KE, Baldock C, Bella J, Boot-Handford RP. Collagens at a glance. *J Cell Sci*. 2007;120:1955-1958.

32. Koo BH, Coe DM, Dixon LJ, Somerville RP, Nelson CM, Wang LW, Young ME, Lindner DJ, Apte SS. ADAMTS9 is a cell-autonomously acting, anti-angiogenic metalloprotease expressed by microvascular endothelial cells. *Am J Pathol*. 176:1494-1504.

33. Lemarchant S, Pruvost M, Montaner J, Emery E, Vivien D, Kanninen K, Koistinaho J. ADAMTS proteoglycanases in the physiological and pathological central nervous system. *J Neuroinflammation*. 3013;10:133.

34. Zimmermann DR, Dours-Zimmermann MT. Extracellular matrix of the central nervous system: from neglect to challenge. *Histochem Cell Biol*. 2008;130:635-653.

Table 1. Gene array results of angiogenesis-related genes in the neurovascular niche

Gene symbol	Gene description	Fold change Tie2-Cre^{ERT2}; Stat3$^{floxed/KO}$ vs Tie2-Cre^{ERT2}	p-value (t-test)	Gene accession
Adamts9	a disintegrin-like and metallopeptidase (reprolysin type) with thrombospondin type 1 motif, 9	5.02	0.00	NM_175314
Sfrp4	secreted frizzled-related protein 4	2.85	0.01	ENSMUST00000169327
Timp1	tissue inhibitor of metalloproteinase 1	2.51	0.00	NM_001044384
Cd36	CD36 antigen	2.47	0.00	NM_001159557
Thbs1	thrombospondin 1	2.02	0.00	NM_011580
Agt	angiotensinogen (serpin peptidase inhibitor, clade A, member 8)	-3.08	0.01	NM_007428
Tnr	tenascin R	-4.80	0.03	NM_022312
Edil3	EGF-like repeats and discoidin I-like domains 3	-4.30	0.01	NM_001037987
Nrxn1	neurexin I	-3.87	0.03	NM_020252
Pcdh10	protocadherin 10	-3.69	0.04	NM_001098171
Cdh19	cadherin 19, type 2	-3.52	0.04	NM_001081386
Nrcam	neuron-glia-CAM-related cell adhesion molecule	-3.10	0.01	NM_176930
Nlgn1	neuroligin 1	-2.96	0.05	NM_138666
Olfm3	olfactomedin 3	-2.39	0.04	NM_153157
Ptk2b	PTK2 protein tyrosine kinase 2 beta	-2.18	0.04	NM_001162365
Prkca	protein kinase C, alpha	-2.09	0.05	NM_011101
Cdh12	cadherin 12	-2.01	0.01	NM_001008420
Apln	apelin	2.19	0.00	NM_013912
Bmp2	bone morphogenetic protein 2	2.63	0.03	NM_007553
Hmox1	heme oxygenase (decycling) 1	3.12	0.00	NM_010442
Pgf	placental growth factor	4.11	0.00	NM_008827
Aplnr	apelin receptor	7.46	0.00	NM_011784
Tnr	tenascin R	-4.80	0.03	NM_022312
Edil3	EGF-like repeats and discoidin I-like domains 3	-4.30	0.01	NM_001037987
Nrxn1	neurexin I	-3.87	0.03	NM_020252
Pcdh10	protocadherin 10	-3.69	0.04	NM_001098171

Anti-angiogenic (rows Adamts9 through Agt); *angiogenic* (rows Tnr through Pcdh10)

Table 2. Gene array results of axonogenesis-related genes in the neurovascular niche

	Gene symbol	Gene description	Fold change Tie2-Cre^{ERT2}; Stat3$^{floxed/KO}$ vs Tie2-Cre^{ERT2}	p-value (t-test)	Gene accession
axon growth promoting	**Kit**	kit oncogene	3.91	0.00	NM_001122733
	Lamb1	laminin B1	2.23	0.02	NM_008482
	Olfm1	olfactomedin 1	-2.00	0.02	NM_019498
	Camk4	calcium/calmodulin-dependent protein kinase IV	-2.04	0.04	NM_009793
	Slitrk4	SLIT and NTRK-like family, member 4	-2.09	0.01	NM_178740
	Prkca	protein kinase C, alpha	-2.09	0.05	NM_011101
	Ntrk3	neurotrophic tyrosine kinase, receptor, type 3	-2.21	0.05	ENSMUST00000039431
	Mtap2	microtubule-associated protein 2	-2.21	0.03	NM_001039934
	Kif5c	kinesin family member 5C	-2.22	0.05	NM_008449
	Unc5a	unc-5 homolog A (C. elegans)	-2.31	0.04	ENSMUST00000026994
	Slitrk1	SLIT and NTRK-like family, member 1	-2.32	0.05	NM_199065
	Chn1	chimerin (chimaerin) 1	-2.44	0.03	NM_001113246
	Pak3	p21 protein (Cdc42/Rac)-activated kinase 3	-2.46	0.03	ENSMUST00000112863
	Ntm	neurotrimin	-2.46	0.04	NM_172290
	Robo2	roundabout homolog 2 (Drosophila)	-2.53	0.01	NM_175549
	Celsr2	cadherin, EGF LAG seven-pass G-type receptor 2 (flamingo homolog, Drosophila)	-2.65	0.03	NM_017392
	Cyfip2	cytoplasmic FMR1 interacting protein 2	-2.79	0.02	NM_133769
	Nlgn1	neuroligin 1	-2.96	0.05	NM_138666
	Chl1	cell adhesion molecule with homology to L1CAM	-2.99	0.02	NM_007697
	Tbr1	T-box brain gene 1	-3.06	0.02	NM_009322
	Nlgn3	neuroligin 3	-3.08	0.02	NM_172932
	Nrcam	neuron-glia-CAM-related cell adhesion molecule	-3.10	0.01	NM_176930
	Mdga2	MAM domain containing glycosylphosphatidylinositol anchor 2	-2.91	0.03	NM_001193266
	Dclk1	doublecortin-like kinase 1	-3.32	0.05	ENSMUST00000167204

Ncam1	neural cell adhesion molecule 1	-3.53	0.02	NM_001081445	
Reln	reelin	-3.65	0.00	NM_011261	
Pcdh10	protocadherin 10	-3.69	0.04	NM_001098171	
Dock3	dedicator of cyto-kinesis 3	-3.78	0.03	NM_153413	
Ptprz1	protein tyrosine phosphatase, receptor type Z, polypeptide 1	-3.91	0.05	NM_001081306	
Slitrk3	SLIT and NTRK-like family, member 3	-3.95	0.03	NM_198864	
Lrrc4c	leucine rich repeat containing 4C	-4.04	0.02	NM_178725	
Bai3	brain-specific angiogenesis inhibitor 3	-4.86	0.04	ENSMUST00000151309	
Axon growth inhibiting **Xylt1**	xylosyltransferase 1	-2.15	0.05	NM_175645	
Pdlim1	PDZ and LIM domain 1 (elfin)	4.07	0.01	NM_016861	

Figure Legends:

Figure 1. Endothelial-specific ablation of Stat3. Endothelial Stat3 ablation was induced in Tie2-Cre^{ERT2};Stat3^{floxed/KO} mice by tamoxifen administration for five consecutive days. Tie2-Cre^{ERT2} littermates with tamoxifen injections served as controls. Mice received a 30 min MCAo 2 days after the last tamoxifen injection. Endothelial Stat3 ablation was confirmed by staining of pStat3 and caveolin-1 4 days or 30 days after the last tamoxifen administration and shown as a ratio to the caveolin positive area **(B)**. Images were taken in 200x magnification in the peri-ischemic subcortical region **(A)**. pStat3 positive and caveolin-1 negative cells **(C)** were counted per view. Scatter dot blots are mean cell counts of triplicate fields per mouse and are presented as mean ± s.d.. Regression analysis with robust variance estimates yielded significant differences between day 2 and day 28 (p<0.001); values for WT mice were significantly higher (p<0.001), and differences between Tie2-Cre^{ERT2} and Tie2-Cre^{ERT2};Stat3^{floxed/KO} were significantly higher at day 28 than at day 2 (interaction: p=0.003). **C:** Number of pStat3 positive and caveolin-1 negative cells. **D:** Expression of Stat3 mRNA of ischemic and contralateral hemispheres of wildtype mice determined by real-Time RT-PCR. Data are presented as mean ± s.d. of 3 – 4 mice or 2 mice (native brains) per time point and group. Stat3 mRNA (log-transformed) after MCAo was tested over time in wildtype mice ipsi/contra with a linear mixed model including an interaction term for time*ipsi/contra to account for clustering of data in mice (random intercept model). **E:** Endothelial Stat3 activation was determined by immunofluorescence co-staining of pStat3 and caveolin-1. The number of pStat3 / caveolin-1 double positive cells was counted and expressed as a ratio of the caveolin-1 positive area and within the peri-infarct region at 2 days and 28 days after ischemia. Unequal variance t-test for independent samples was used. *p < 0.001 for B, D and E.

Figure 2. Endothelial Stat3 ablation has no effect on ischemic lesion volume 2 days after cerebral ischemia. Tie2-Cre^{ERT2} littermates (n=23) and Tie2-Cre^{ERT2};Stat3$^{floxed/KO}$ (n=16) mice received tamoxifen on five consecutive days followed after a 2 day interval by a 30 min MCAo. **A:** Timeline of experimental setup. **B-C:** Ischemic lesion size was determined by MRI after 2 days. **D-E:** A subset of each genotype (n=12 for Tie2-Cre^{ERT2} littermates, n=9 for Tie2-Cre^{ERT2};Stat3$^{floxed/KO}$) was killed at this time point for lesion volume analysis by NeuN-DAB staining**.** There was no difference in lesion volume between the two groups two days after cerebral ischemia. Data are presented as scatter dot plots with mean ± s.d. and analyzed by two-tailed Student's t-test (p = 0.25 and p = 0.19, respectively). *p < 0.05 and **p < 0.01 in B-D.

Figure 3. Endothelial-specific ablation of Stat3 increases lesion volume 28 days after cerebral ischemia and impairs functional outcome 14 days after cerebral ischemia. Tie2-Cre^{ERT2} littermates (n=11) and Tie2-Cre^{ERT2};Stat3$^{floxed/KO}$ (n=7) were subjected to 30 min MCAo after 5 days of daily tamoxifen administration followed by an interval of 2 days, and were killed at 28 days after the onset of cerebral ischemia. Lesion volume was determined by NeuN-DAB staining **(A-B)**. Data are presented as scatter dot plots with mean ± s.d. and analyzed by two-tailed Student's t-test with p = 0.01 versus littermates. **C:** Rotarod. Data are presented as bar graphs with mean ± s.d and analyzed by two-tailed Student's t-test with p = 0.04 versus littermates (Tie2-Cre^{ERT2} littermates n=12, Tie2-Cre^{ERT2};Stat3$^{floxed/KO}$ n=12). **D:** extended neuroscore. Data are analyzed by Mann-Whitney U test with p = 0.03 (Tie2-Cre^{ERT2} littermates n=12, Tie2-Cre^{ERT2};Stat3$^{floxed/KO}$ n=12).

Figure 4. Post-ischemic angiogenesis is reduced after endothelial-specific ablation of Stat3 and

microglia proliferation is increased. Tie2-Cre[ERT2] littermates (n=11) and Tie2-Cre[ERT2];Stat3[floxed/KO] (n=7) were subjected to 30 min MCAo after 5 days of daily tamoxifen administration followed by a free interval of 2 days and were killed 28 days after cerebral ischemia and stained for caveolin-1. **A:** Multiple image alignment of caveolin-1 stained brain. **C:** The caveolin-1 positive area above a preset threshold was determined using semiautomatic software algorithms and presented as a ratio of ipsilateral and contralateral hemispheres. Data are presented as scatter dot blots with mean ± s.d. and analyzed using two-tailed Student's t-test with $p = 0.01$. **B:** Ischemic hemispheres were stained for caveolin-1 and anti-BrdU. **D:** Vessel associated BrdU double positive cells (caveolin-1+/BrdU+) were counted per mm^2 and presented as scatter dot plots with mean ± s.d. and analyzed using two-tailed Student's t-test with $p = 0.003$. **E-F:** 3D projections of peri-infarct vascular networks. **G-H:** FACS analysis of the numbers of CD11b$^+$/CD45^{low} (microglia) and CD11b$^+$/CD45^{high} (monocytes) 4 days after ischemia. The percentage of microglia is increased 4 days after ischemia in the ischemic hemisphere, and the increase is significantly higher after endothelial Stat3 ablation. FACS data were analyzed with a linear mixed model using FACS as dependent variable (log-transformed) and genotype, CD11b$^+$/CD45^{low}/CD11b$^+$/CD45^{high} and ipsilateral/contralateral as independent variables. In the model we also included interaction terms for genotype*ipsi/contra and CD11b$^+$/CD45^{low}/CD11b$^+$/CD45^{high}*genotype. All p-values (*< 0.05; **< 0.01, and ***< 0.001) reported are derived from regression based post hoc tests using Bonferroni-adjustment for multiple testing.

Figure 5. Endothelial Stat3 ablation leads to an anti-angiogenic and axon-growth inhibiting micro-milieu within the neurovascular niche. Tie2-Cre[ERT2] littermates and Tie2-

Cre^{ERT2};Stat3$^{floxed/KO}$ were subjected to 30 min MCAo after 5 days of daily tamoxifen administration followed by a free interval of 2 days, and were killed 4 days after cerebral ischemia. CD31-enriched cells were isolated and a gene array performed (n=3; total number of animals per genotype=21 with 7 animals pooled for enrichment). **A:** Staining of cytospins of CD31-MACS sorted cells with caveolin-1 and DAPI. **B:** Expression levels of marker genes specific for endothelial cells, neurons, astrocytes or oligodendrocytes. Fold expression of angiogenesis-related **(C)** and axon growth-related **(D)** genes compared between Tie2-Cre^{ERT2};Stat3$^{floxed/KO}$ and Tie2-Cre^{ERT2} littermates. For testing expression levels of angiogenic or axon-modulating genes between WT and KO we used one sample t-test to test fold_mRNA against the hypotheses that these values are 0 on average. For anti-angiogenic genes the fold change was on average 2.0 (p=0.133); for angiogenic genes it was -1.6 (p=0.054), for axon growth promoting genes it was -2.5 (p<0.001) and for axon growth inhibiting genes it was 0.6 (p=0.884).

Figure 6. Endothelial Stat3 ablation increases Adamts9 and extracellular matrix glycosylation. Tie2-Cre^{ERT2} littermates (n=11) and Tie2-Cre^{ERT2};Stat3$^{floxed/KO}$ mice (n=7) were subjected to 30 minute MCAo after 5 days of daily tamoxifen administration followed by a free interval of 2 days and were killed 4 days **(A)** or 28 days **(B, C)** after ischemia. **A:** Staining of Adamts9 and caveolin-1. 4 days after ischemia Adamts9 is mainly expressed in endothelial cells. **(B-C):** Staining of cryosections 28 days after ischemia with isolectin-B4. Isolectin-B4 stains components of the ECM in the ischemic hemisphere. The isolectin-B4 positive volume is increased after endothelial Stat3 ablation. *p < 0.05.
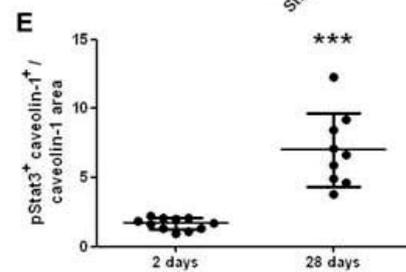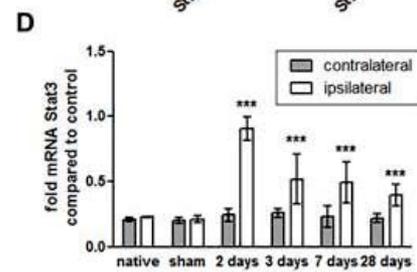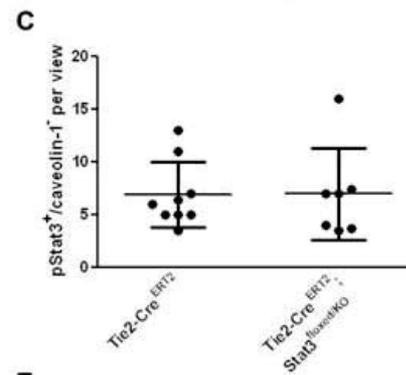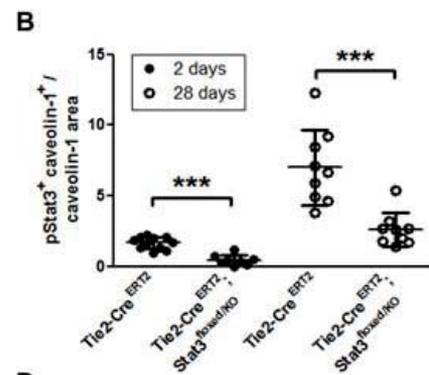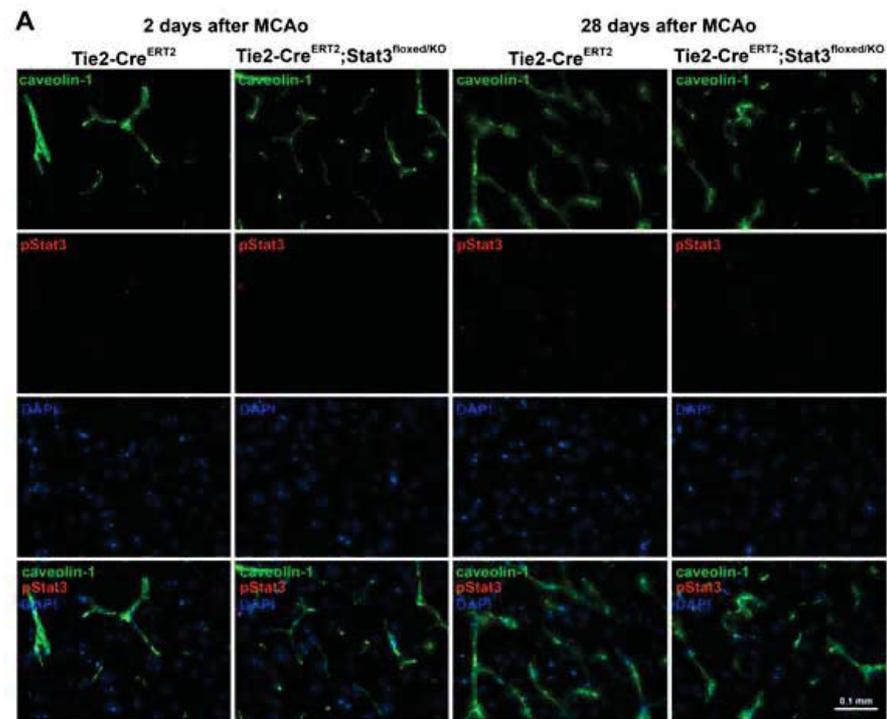
Figure 1
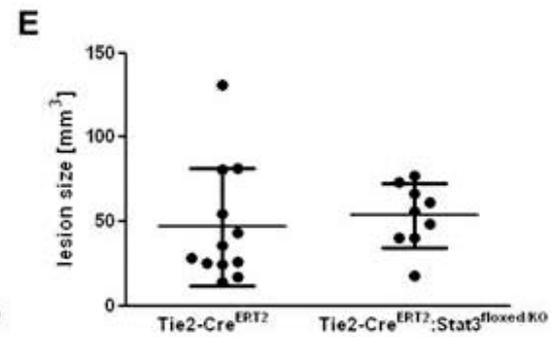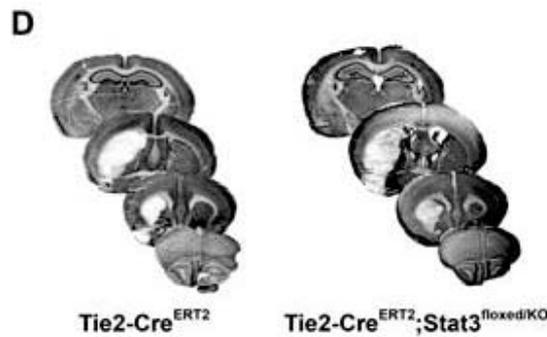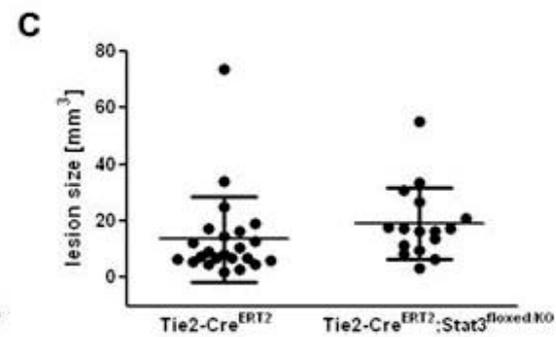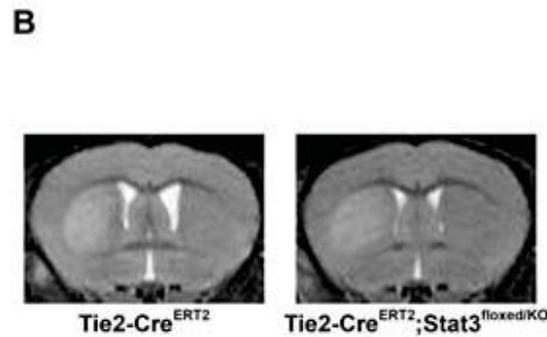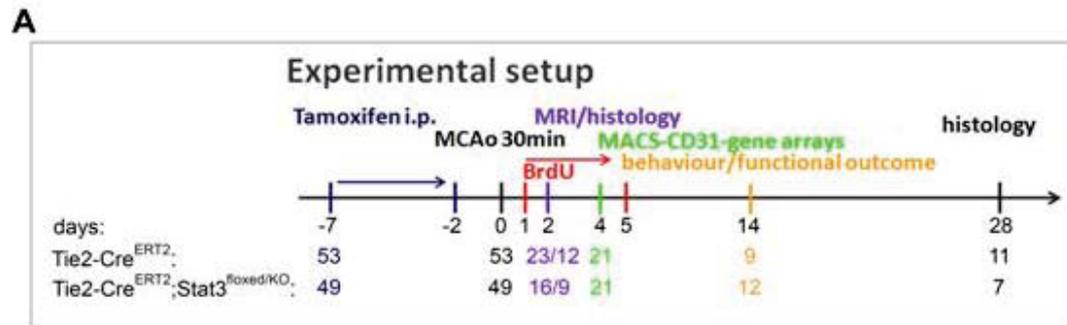
Figure 2
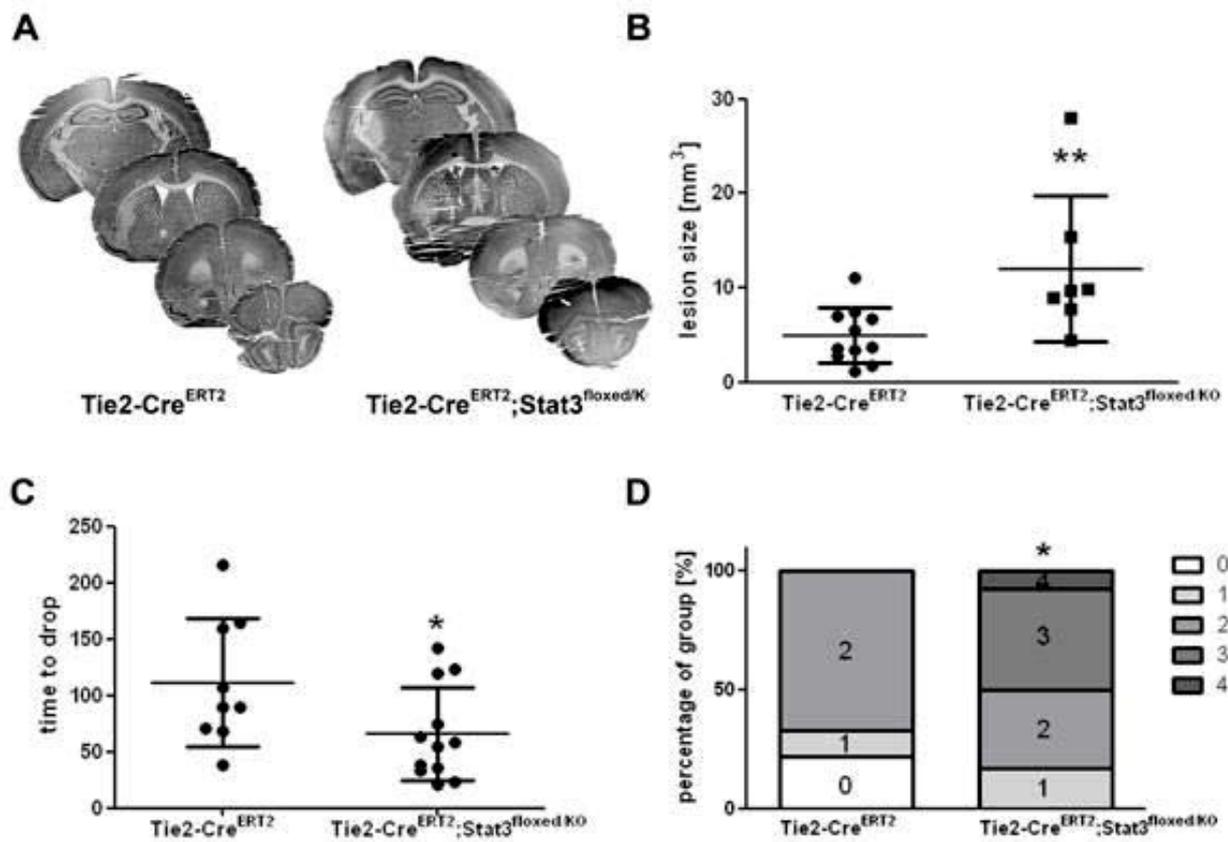
Figure 3

Figure 4

Figure 5

A

Adamts9

caveolin-1

caveolin-1
Adamts9

0.5 mm

B

Tie2-Cre^{ERT2}

Tie2-Cre^{ERT2};Stat3$^{floxed/KO}$

C

isolectin-B4 volume [mm^3]

Tie2-Cre^{ERT2} Tie2-Cre^{ERT2};Stat3$^{floxed/KO}$
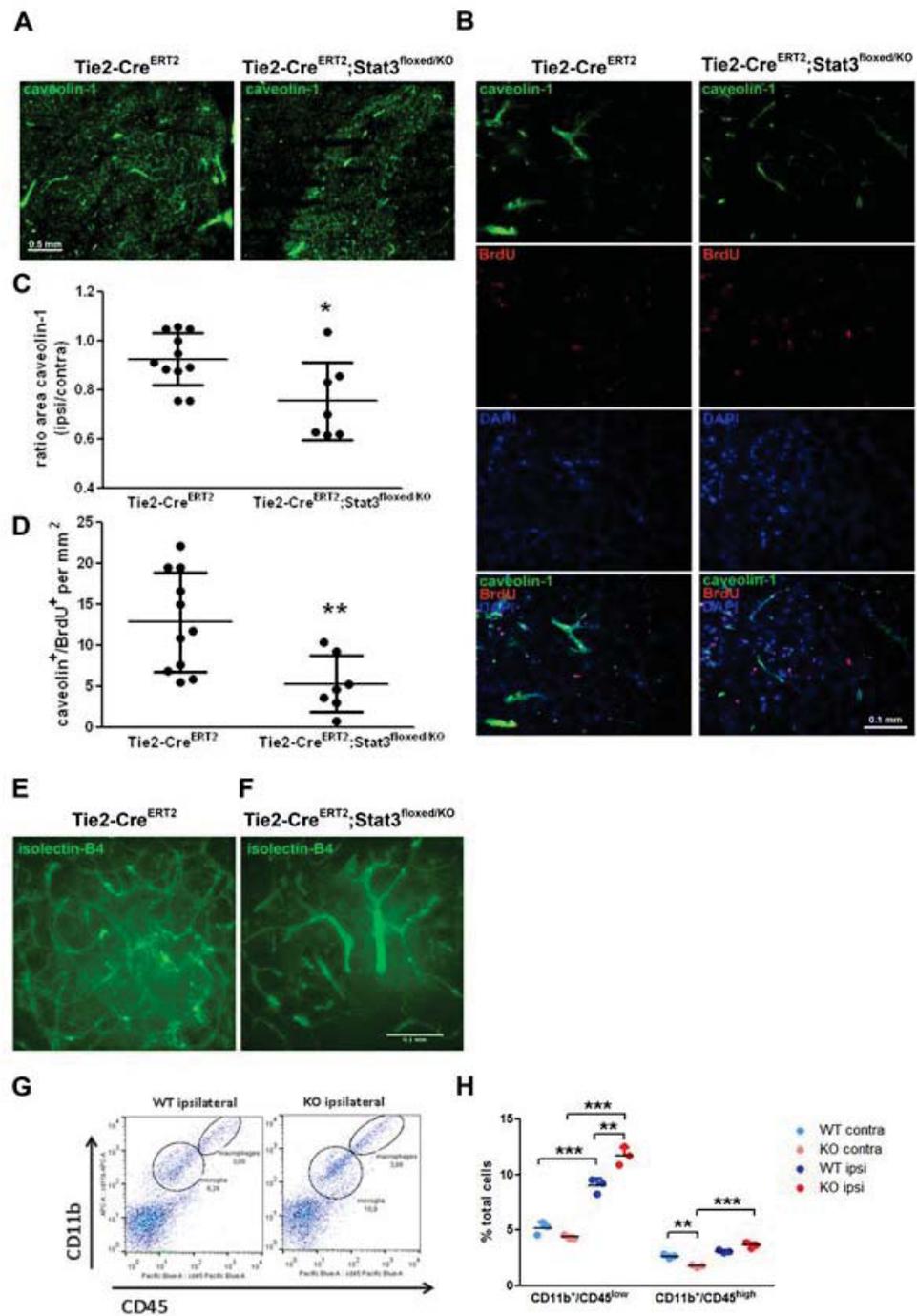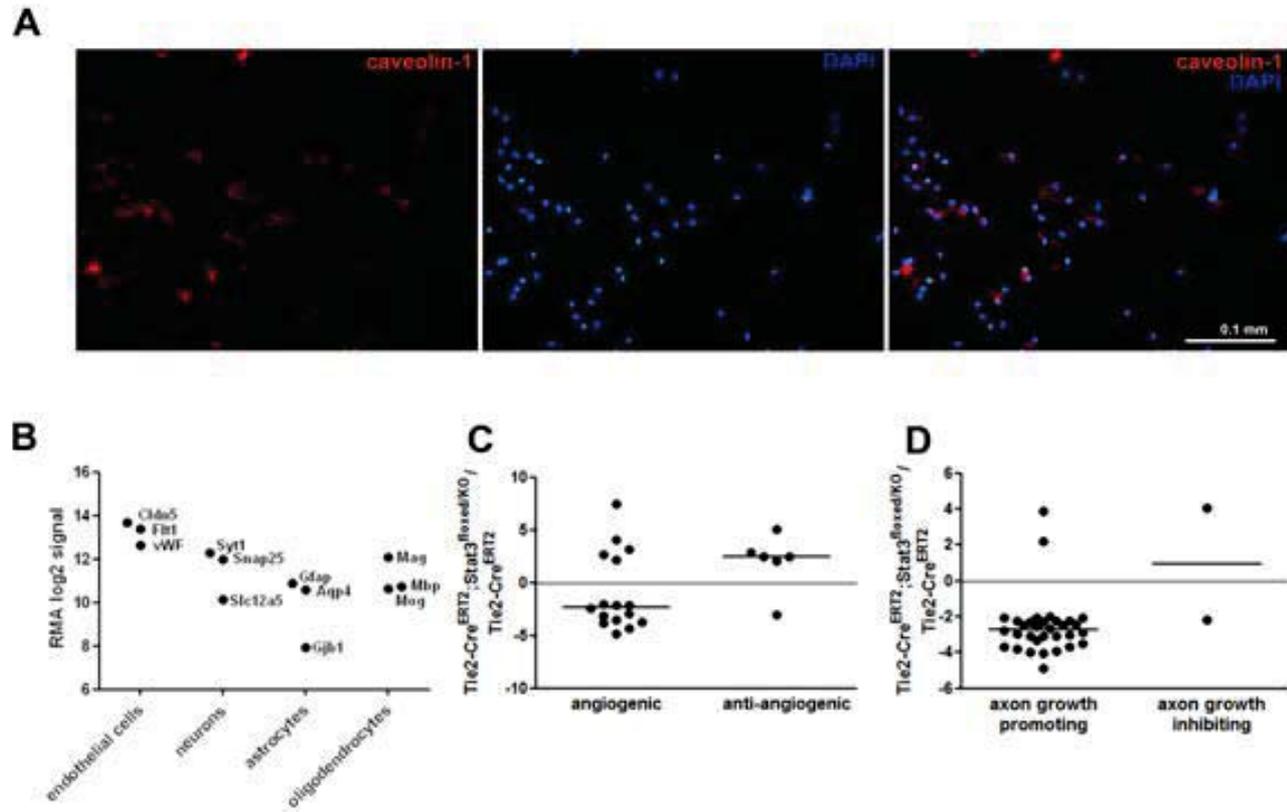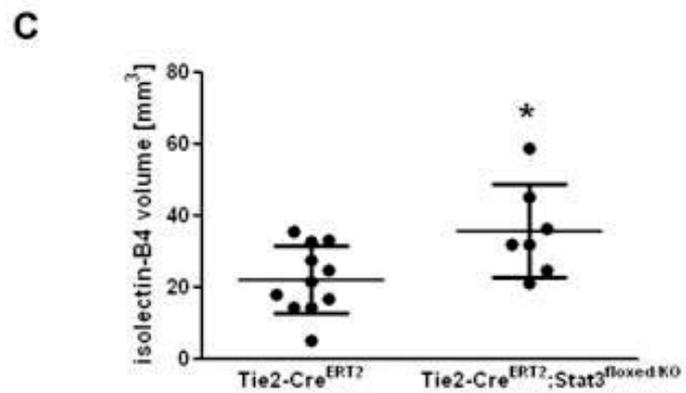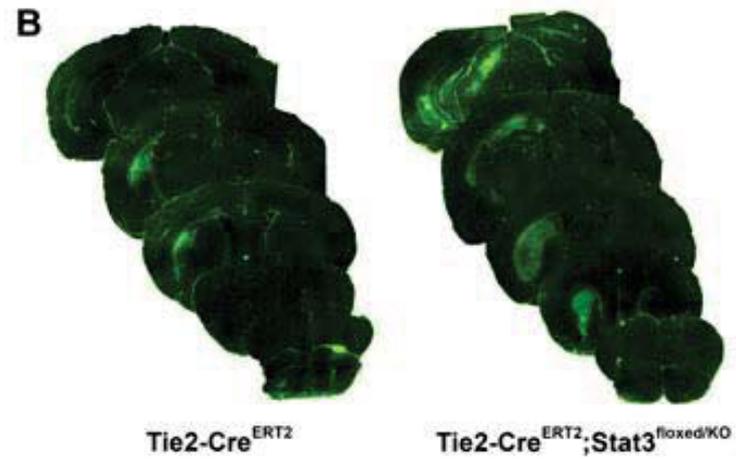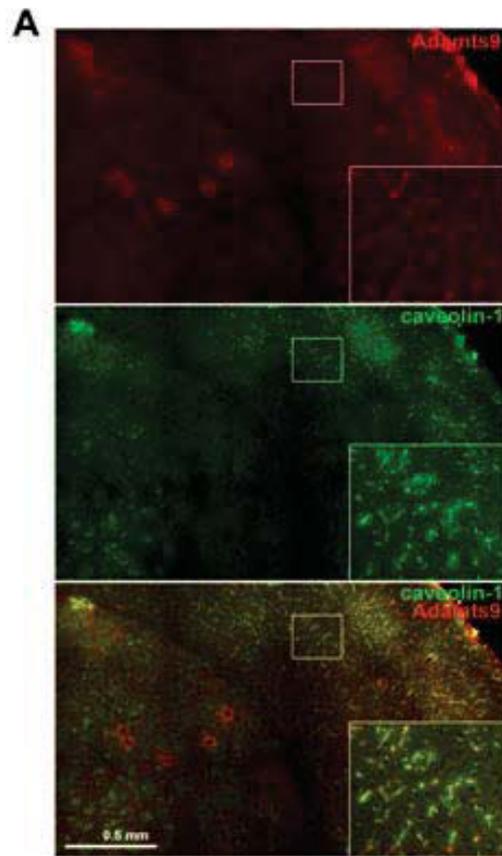
Figure 6

SUPPLEMENTAL MATERIAL

Supplemental Methods

Animals and treatments

All animal experiments were approved by the local governmental authorities (Landesamt für Gesundheit und Soziales, G0354/11). Mice had access to food and water ad libitum and were kept under a 12 hours light and dark cycle. Stat3[floxed/KO] mice[1] were crossbred with Tie2-Cre[ERT2] mice.[2] Both transgenic mouse lines were backcrossed onto a C57Bl/6_N background and littermates were used for the experiments. Mice were genotyped by standard polymerase chain reaction protocols. Endothelial specific knock out of Stat3 was induced by a 5 day i.p. application of Tamoxifen (1 mg/d) which results in an excision of exon 22 that codes for the domain including tyrosine 705 (Y705) which is phosphorylated for activation of Stat3. Tie2-Cre[ERT2] littermates served as control group. The concealment to the genotypes was blinded throughout the entire experiment and histological analysis. Scientists were blinded to the allocation of the mice to the groups. Litters were caged in mixed groups after heterozygous breeding and undergone surgery after randomization. Animals for experiments were gender and age matched. Tie2-Cre[ERT2] littermates and Tie2-Cre[ERT2];Stat3[floxed/KO] mice were 4.8 ± 1.8 and 4.6 ± 1.6 month old. The sex ratio between Tie2-Cre[ERT2] littermates and Tie2-Cre[ERT2];Stat3[floxed/KO] mice did not differ as analyzed using Fisher's Exact test. Endothelial specific knock out of Stat3 was confirmed by immunofluorescence staining of phosphorylated Stat3 (Y705). Mice received BrdU (50 µg/g body weight) i.p. from day 2-7 after MCAo at a concentration of 10 mg/ml. 3 animals in total were excluded from the study due to the lack of a lesion while two of them being Tie2-Cre[ERT2] littermates and 1 Tie2-Cre[ERT2];Stat3[floxed/KO].

Model of middle cerebral artery occlusion (MCAo)

Filamentous middle cerebral artery occlusion of the left side was performed for 30 minutes with indicated reperfusion time points according to the published standard operating procedure in our laboratory.[3] In brief, mice were anesthetized with 1.0% isofluorane in a mixture of 70% vol/vol N_2O and 30% vol/vol O_2 using a vaporizer and face mask. Brain ischemia was induced with an 8.0 nylon monofilament coated with a silicone resin /hardener mixture (Xantopren M Mucosa and Activator NF Optosil Xantopren, Haereus Kulzer, Germany) as described. The filament was introduced into the left internal carotid artery up to the anterior cerebral artery. Thereby, the middle cerebral artery and anterior choroidal arteries were occluded. Filaments were withdrawn after 30 min to allow reperfusion.

RNA-isolation

Mice were deeply anesthetized, cardially perfused with NaCl-solution, decapitated and the brain removed after 2, 3, 7, and 28 days of reperfusion. The brains were cut in 1 mm coronal slices using a brain matrix. In the slices ischemic and contralateral hemispheres were separated and snap frozen and pestled in liquid nitrogen, homogenized using a Dounce homogenizer and RNA was extracted using Trizol (Invitrogen). RNA was stored at -80 °C prior to transcription.

Real-time RT-PCR

1 µg of RNA was transcribed with MLV-reverse transcriptase (Promega) using random primers (Roche) and oligo-dT primers (Eurofins-MWG). Real-time PCR was performed with intron spanning primers for Ywhaz and Sdha as internal controls and primers for Stat3 using Sybr green (Qiagen). Comparable primer efficiency was confirmed. For all runs melting curves were analyzed. No template and untranscribed RNA served as negative controls. Fold-amount of mRNA compared to mean of internal controls was calculated using the equation: $2^{-(Ct(gene\ of\ interest)-Ct(internal\ control))}$

Histology and immunofluorescence

Mice were deeply anesthetized, cardially perfused with NaCl-solution, decapitated, and brains snap frozen in -40 °C isopentane for cryostat sectioning at 2 and 28 days after MCAo. 20 µm cryosections were fixed with Aceton/Methanol for 10 min at -20 °C and washed 3 times for 5 min with PBS. Sections that were stained for caveolin-1 (B&D) or pStat3 (Tyr705) (Cell signaling) were blocked in PBS with 10 % normal goat serum and 0.1 % Triton for 1 h and incubated with caveolin-1 (1:100, BD), Adamts9 (1:50; Santa Cruz) or pStat3 (1:50, Cell signaling) antibodies over night, washed 2 times with PBS, incubated with goat anti-mouse antibody (1:400, conjugated with Alexa 488) or goat anti-rabbit antibody (1:400, conjugated with Alexa 594) for 2 h, washed 2 times for 5 min with PBS, incubated 3 min with DAPI, washed 2 times with water and mounted with immunomount (GeneTex). Sections that were stained for BrdU were incubated with 2 N HCl for 30 min at 37 °C followed by an incubation in 0.1 M borate buffer for 10 min at room temperature, washed 6 times for 10 min with TBS, blocked in TBS with 10 % normal goat serum and 0.1 % Triton for 30 min, incubated with primary antibody against BrdU (1:100, AbD Serotec) in TBS with 1 % normal goat serum and 0.1 % Triton over night, washed 2 times for 5 min with TBS and 1 time for 15 min with TBS with 1 % normal goat serum and 0.1 % Triton, incubated with secondary antibody (1:400) for 2 h washed 2 times for 5 min with PBS, incubated 3 min with DAPI, washed 2 times with water and mounted with immunomount (GeneTex). Sections stained for NeuN were incubated with 0.3 % H_2O_2, washed 3 times for 5 min with PBS, blocked in PBS with 1 % normal goat serum and 0.1 % Triton for 30 min, incubated wit anti-NeuN-biotin antibody (1:100, Chemicon (Millipore)) over night, washed 3 times for 5 min with PBS, incubated with VECTASTAIN Elite ABC-kit reagent (Vector labs) for 1 h, washed 3 times for 5 min with PBS, incubated with Vector DAB substrate (Vector labs) for 10 min, washed 3 times for 5 min with water, dehydrated with ethanol, incubated with Rotihistol (Carl Roth) and mounted with Vitroclud (R. Langenbrinck, Labor- und Medizintechnik).

For orthogonal projections, brains were perfused with NaCl-solution with subsequent 4% PFA perfusion, and brains were vibratome-sliced into frontal 500 µm sections, incubated with isolectin-B4 (Griffonia simplicifolia) conjugated to Alexa Fluor 594 (Life Technologies, Carlsbad, Germany) without further permeabilization to specifically label the blood vessel network. In addition, the slices were optically cleared with a solution consisting of 4 M urea, 10% glycerol (v/v), 0.1% TritonX-100 (v/v) for 2 days.

Microscopy

Widefield fluorescence microscopic images were collected using an Olympus IX81 inverted microscope equipped with a MT10 illumination system, a CCD camera (Hamamatsu, Ammersee, Germany) and a Scan FM table (Maerzhaeuser, Wetzlar, Germany) for automated image acquisition under the control of Xcellence software (Olympus, Hamburg, Germany). For whole brain slice images (multiple image alignments) UPlan FLN 4x and for all other images LCACHN 20x were used.

Confocal images of isolectin B4 stained vascular networks were collected with a spinning disc system consisting of a Axio Observer Z.1 microscope (Zeiss, Jena, Germany) equipped with a Yokogawa CSU-X1 unit using a 20x/0.4 Korr M27 objective and processed with ZEN2012 software (Zeiss, Jena, Germany). Orthogonal projections (60 µm) and supplementary movie were generated by ImageJ.

Lesion volume determination and behavioral tests

Cerebral lesion volume was quantified with ImageJ analysis software (NIH, USA) on 20 µm NeuN-DAB-stained cryostat sections and calculated by summing the infarct sizes of each section as described previously.[3] To assess motor coordination, a Rotarod test was used (TSE Sytems). Mice were placed on an accelerating rotating rod (acceleration from 2 rpm to 40 rpm within 5 min) and a stop-clock was started. When the mice dropped and touched the sensing platform below, the stop-clock stopped automatically. Each animal performed three trials.

An extended neuroscore that consisted of several components was performed. The first component was a modified Bederson score that provided a quick overall assessment of the activity and locomotor capabilities of the mouse with a score of 0 indicating normal spontaneous movement, a score of 4 indicating no movement, and circling behaviours or forelimb flexion making up the middle range of the score.[4] The next three components consisted of 3 point score hand tests. The first two require that the mouse be lowered by the base of the tail towards the lid of the home cage. A mouse would score 0 (normal postural reflex) if both forelimbs were extended, while a score of 2 would be assigned for asymmetrical forelimb extension or curved body posture. An animal would score 0 on the third component (normal forelimb grasping reflex) if both forelimbs grasped the lid of the home cage, versus 1 for asymmetrical grasping, or 2 for no grasping. Finally, the vertical screen test was conducted in which the animal was placed on the lid of the home cage and the lid was gently tilted to a 90° angle. A score of 0 would indicate normal locomotor behaviour as the mouse would hang on and climb around, whereas a score of 2 indicates the inability to remain on the lid, or jumping off. A composite score was determined for each mouse at each timepoint.

For lesion size determination a total number of 16 endothelial-Tie2-Cre^{ERT2};Stat3$^{floxed/KO}$ and 23 wildtype littermates were used. All underwent MRI at 2 days after ischemia. A subset of 9 endothelial-Tie2-Cre^{ERT2};Stat3$^{floxed/KO}$ and 12 wildtype littermates were killed at 2 days after ischemia and a subset of 7 endothelial-Tie2-Cre^{ERT2};Stat3$^{floxed/KO}$ and 11 wildtype littermates at 28 days for histological lesion size determination. For behavioral tests 12 endothelial-Tie2-Cre^{ERT2};Stat3$^{floxed/KO}$ and 12 wildtype littermates were used.

MRI

Magnet resonance imaging (MRI) was performed using a 7 Tesla rodent scanner (Pharmascan 70 ∕ 16AS) with a 16 cm horizontal bore magnet and a 9 cm (inner diameter) shielded gradient with an H-resonance-frequency of 300 MHz and a maximum gradient

strength of 300 mT/m. For imaging a [1]H-RF quadratur-volume resonator with an inner diameter of 20 mm was used. Data acquisition and image processing were carried out with the Bruker software Paravision 4.0. During the examinations mice were placed on a heated circulating water blanket to ensure constant body temperature of 37 °C. Anaesthesia was induced with 2.5% and maintained with 1.0–2.0% isoflurane delivered in an O_2/N_2O mixture (30/70%) via a facemask under constant ventilation monitoring. A RARE-T2-weighted sequence was used. Imaging parameters: for T2 TR / TE = 4200 / 36 ms, RARE factor 8, 4 averages). 20 axial slices with a slice thickness of 0.5 mm, a field of view of 2.75 x 2.75 cm and a matrix of 256 x 256 were positioned over the brain excluding olfactory bulb. Data evaluation was performed with Analyse 5.0.

For stroke volumetry the hyperintense areas of ischemic tissue in T2-weighted images were assigned with a region of interest tool (ROI). This enables a threshold-based segmentation by connecting all pixels within a specified threshold range about the selected seed pixel and results in a 3D object map of the whole stroke region. Further the total volume of the whole object map was automatically calculated.

Vessel density determination by immunofluorescence

Vessels were stained with anti-caveolin-1 antibodies and images of the brain section containing the ischemic area were taken in 40x magnification and aligned to a multiple image alignment (MIA) of the complete brain section. The area stained for caveolin-1 was determined using ImageJ software by selecting a constant color threshold for all MIAs. The ratio of the area of caveolin-1 on the ischemic hemisphere to the area on the contralateral hemisphere was calculated to normalize the values for different brain sizes. In addition caveolin-1 and BrdU double positive cells were counted.

ELISA

ELISA assays for determining Vegf (R&D systems) and Il6 (Invitrogen) levels were performed according to manufacturer's instructions.

Isolation of CD31-enriched cells

Mice were euthanized 4 days after cerebral ischemia by i.p. injection of 200 µl pentobarbital-sodium (Narcoren, Pharmazeutischen Handelsgesellschaft) and perfused using a 0.9 % NaCl solution. The brain was extracted and stored in ice-cold HBSS (Gibco-Invitrogen). The olfactory bulbs and the cerebellum were cut by a scalpel and discarded. The ipsi- and contralateral hemispheres were divided and processed separately. Hemispheres from 6-8 animals were pooled.

The tissue was dissociated using the Papain Neural Tissue Dissociation Kit (Miltenyi Biotec, Bergisch-Gladbach, Germany) according to the manufacturer's instructions. To remove the myelin we followed a protocol published elsewhere.[5] In brief, per one hemisphere the brain cell suspension was mixed with a total of 25 ml of a 22 % Percoll (Th.Geyer, Renningen, Germany) solution and a layer of 5 ml cold PBS (Gibco-Invitrogen) was added on top. Centrifugation at 950 g with slow acceleration and without breaks created a gradient that separated the cell pellet on the bottom of the tube from the myelin which was carefully aspirated. The cell pellet was resuspended in sorting buffer for subsequent magnetic-activated cell sorting (MACS) or flow cytometry analysis. A total number of 21 endothelial-Tie2-Cre[ERT2];Stat3[floxed/KO] and 21 wildtype littermates were used and divided to 3 groups each before isolation.

MACS sorting

The CD31+ samples for the microarray were generated using MACS. Following percoll gradient centrifugation, cell pellets were resuspended in PBS, containing 0.5% FCS and 2

mM EDTA and labeled with anti-CD31 microbeads™ (Miltenyi Biotec, 130-097-418). The MACS isolation was carried out according to the manufacturer's instructions and cells were subsequently used for RNA isolation. Purity of CD31+ sorted cells was assessed by flow cytometry and cytospin. For cytospin, 50,000 MACS-sorted cells in 100 µl were centrifuged onto glass slides for 5 min at 650 rpm using a Shandon Cytospin 3 cyto-centrifuge. Total RNA from MACS or FACS-sorted cells was isolated using the RNeasy Plus Mini Kit (Qiagen, Hilden, Germany). Total RNA was eluted in RNase-free water and RNA yield was measured using a Nanodrop 1000 (Nanodrop, Wilmington, DE, USA) spectrophotometer and quality was assessed using an Agilent 2100 Bioanalyzer (Agilent, Santa Clara, CA, USA). Samples were stored at -80 °C until further use.

GeneChip microarray assay

Sample preparation for microarray hybridization was carried out as described in the Ambion WT Expression Kit Protocol (Life Technologies, Carlsbad, CA, USA) and the Affymetrix WT Terminal Labeling and Hybridization User Manual (Affymetrix, Inc., Santa Clara, CA, USA).

In brief, 300 ng of total RNA were used to generate double-stranded cDNA. 12 µg of subsequently synthesized cRNA was purified and reverse transcribed into sense-strand (ss) cDNA, whereat unnatural dUTP residues were incorporated. Purified ss cDNA was fragmented using a combination of uracil DNA glycosylase (UDG) and apurinic/apyrimidinic endonuclease 1 (APE 1) followed by a terminal labeling with biotin. 3,8 µg fragmented and labeled ss cDNA were hybridized to Affymetrix Mouse Gene 1.0 ST arrays for 16 h at 45 °C in a rotating chamber. Hybridized arrays were washed and stained in an Affymetrix Fluidics Station FS450, and the fluorescent signals were measured with an Affymetrix GeneChip Scanner 3000 7G.

Sample processing was performed at an Affymetrix Service Provider and Core Facility, "KFB - Center of Excellence for Fluorescent Bioanalytics" (Regensburg, Germany; www.kfb-regensburg.de).

Microarray data analysis

Summarized probe set signals were calculated by using the RMA[6] algorithm with the Affymetrix GeneChip Expression Console Software. After exporting into Microsoft Excel, average signal values, comparison fold changes and significance P values were calculated using unequal variance Student's t test. Probe sets with a fold change above 2.0 fold and a p-value lower than 0.05 were considered as significantly regulated.

FACS

For FACS analysis, a sample of each single cell suspension (200 µl) after tissue dissociation and before MACS analysis was transferred into round bottom FACS tubes followed by a washing step with 3 ml FACS buffer (PBS, 1 % BSA, 0.1 % EDTA). After centrifugation cells were re-suspended in 50 µl FACS buffer containing the antibody mix. For determination of the auto fluorescence of the cells, one sample of unstained cells was set aside and staining controls with respective isotypes were prepared by splitting the samples before staining. The FACS analyzer was calibrated using BD™Calibrite beads followed by the automated compensation program. To distinguish between resident microglia and invading macrophages, we used the markers CD11b-APC and CD45-efluor™450 for FACS analysis (all antibodies from eBioscience, San Diego, CA). The percentage of positive cells determined over 10,000 events were analyzed on a BD Biosciences LSR Fortessa 5 Laser analyzer and fluorescence intensity is expressed in arbitrary units on a logarithmic scale. Co-expression of anti-mouse CD11b-APC and CD45-efluor™450 are shown in density plots.

CD11b$^+$CD45^{hi} cells are infiltrating monocytes/macrophages while CD11b$^+$CD45^{low} are the intrinsic microglial population. Data are presented as mean +/- SD, n = 3.

Statistical analysis

All data are presented as scatter dot blots with mean ± standard deviation. The sex ratio was tested using Fisher's exact test. All data were analyzed using unpaired two-tailed Students t-Test. Deviation from normal distribution was checked with histograms and calculation of skewness. In case of an absolute value of the skewness lower one we treated the data as sufficiently normally distributed with regard to statistical methods which require normal distributed data. In case of skewness we log-transformed the data before analyses or used non-parametric methods. Unequal variance t-test for independent samples was used for gene expression analysis and if indicated (Figure 1e). Data of the extended neuroscore were tested using the Whitney-Mann-U-test.

For the test of endothelial specific ablation of Stat3 we used regression analysis with robust variance estimates to overcome the problem of unequal variances with day, genotype and the interaction of both as independent variables.

Stat3 mRNA (log-transformed) after MCAo over time in wildtype mice ipsi/contra was tested with a linear mixed model including interaction term for time*ipsi/contra to account for clustering of data within mice (random intercept model). FACS data were analyzed similarly with a linear mixed model using FACS as dependent variable (log-transformed) and genotype, CD11b$^+$/CD45^{low}/CD11b$^+$/CD45^{high} and ipsilateral/contralateral as independent variables. In the model we also included interaction terms for genotype*ipsi/contra and CD11b$^+$/CD45^{low}/CD11b$^+$/CD45^{high}*genotype. All reported p-values are derived from regression based post hoc tests using Bonferroni-adjustment for multiple testing. Bonferroni adjustment was done for post-hoc tests in a particular regression model. Otherwise no adjustment for multiple testing was applied since this an exploratory study.

For testing expression levels of angiogenic or axon-modulating genes between WT and KO we used one sample t-test to test fold_mRNA against the hypotheses that these values are 0 on average.

Regression models, unequal variance t-test and one sample t-test were calculated using IBM SPSS 22.0. The regression model with robust variance estimates was calculated using STATA/IC 13.1.

Supplemental Table 1. Gene array results of the neurovascular niche after cerebral ischemia

Gene symbol	Gene description	Fold change Tie2-Cre[ERT2]; Stat3[floxed/KO] vs Tie2-Cre[ERT2]	p-value (t-test)	Gene accession
2810055G20Rik	RIKEN cDNA 2810055G20 gene	-2.08	0.05	NR_015543
2810417H13Rik	RIKEN cDNA 2810417H13 gene	2.00	0.01	NM_026515
2900055J20Rik	RIKEN cDNA 2900055J20 gene	-2.22	0.05	NR_045177
4933409K07Rik	RIKEN cDNA 4933409K07 gene	2.40	0.01	NR_033123
6430704M03Rik	RIKEN cDNA 6430704M03 gene	-3.31	0.03	NM_001142965
AA467197	expressed sequence AA467197	4.72	0.00	ENSMUST00000047498
Abcg4	ATP-binding cassette, sub-family G (WHITE), member 4	-2.02	0.04	ENSMUST00000034648
Adam22	a disintegrin and metallopeptidase domain 22	-2.77	0.04	ENSMUST00000088746
Adam23	a disintegrin and metallopeptidase domain 23	-2.89	0.05	NM_011780
Adamts9	a disintegrin-like and metallopeptidase (reprolysin type) with thrombospondin type 1 motif, 9	5.02	0.00	NM_175314
Adcy2	adenylate cyclase 2	-2.90	0.05	NM_153534
Adcy8	adenylate cyclase 8	-2.40	0.04	NM_009623
Adcyap1r1	adenylate cyclase activating polypeptide 1 receptor 1	-2.51	0.04	NM_007407
Adora1	adenosine A1 receptor	-2.52	0.05	NM_001008533
Agt	angiotensinogen (serpin peptidase inhibitor, clade A, member 8)	-3.08	0.01	NM_007428
Agxt2l1	alanine-glyoxylate aminotransferase 2-like 1	-2.43	0.03	NM_027907
AI504432	expressed sequence AI504432	-2.05	0.04	NR_033498
Akap6	A kinase (PRKA) anchor protein 6	-3.38	0.03	NM_198111
Akr1b8	aldo-keto reductase family 1, member B8	2.89	0.00	NM_008012
Amph	amphiphysin	-2.76	0.05	NM_175007

Ank2	ankyrin 2, brain	-2.57	0.04	ENSMUST00000043741
Ano3	anoctamin 3	-3.20	0.02	NM_001128103
Apln	apelin	2.19	0.00	NM_013912
Aplnr	apelin receptor	7.46	0.00	NM_011784
Arhgap32	Rho GTPase activating protein 32	-2.13	0.02	NM_001195632
Astn1	astrotactin 1	-3.70	0.03	NM_001205204
Atp1a3	ATPase, Na+/K+ transporting, alpha 3 polypeptide	-4.24	0.01	NM_144921
B3galt2	UDP-Gal:betaGlcNAc beta 1,3-galactosyltransferase, polypeptide 2	-3.54	0.02	NM_020025
Bai3	brain-specific angiogenesis inhibitor 3	-4.86	0.04	ENSMUST00000151309
Bcl6b	B cell CLL/lymphoma 6, member B	2.12	0.00	NM_007528
Bmp2	bone morphogenetic protein 2	2.63	0.03	NM_007553
C1ql3	C1q-like 3	-3.82	0.03	NM_153155
Cacna2d1	calcium channel, voltage-dependent, alpha2/delta subunit 1	-2.45	0.04	NM_001110843
Cacng2	calcium channel, voltage-dependent, gamma subunit 2	-2.02	0.03	ENSMUST00000019290
Caln1	calneuron 1	-2.45	0.01	NM_181045
Camk4	calcium/calmodulin-dependent protein kinase IV	-2.04	0.04	NM_009793
Camta1	calmodulin binding transcription activator 1	-3.41	0.02	NM_001081557
Car13	carbonic anhydrase 13	2.05	0.03	NM_024495
Cck	cholecystokinin	-3.28	0.01	NM_031161
Ccna2	cyclin A2	2.23	0.01	NM_009828
Ccnb2	cyclin B2	2.08	0.01	NM_007630
Cd14	CD14 antigen	2.12	0.00	NM_009841
Cd36	CD36 antigen	2.47	0.00	NM_001159557
Cda	cytidine deaminase	2.04	0.02	NM_028176
Cdh10	cadherin 10	-3.76	0.05	NM_009865
Cdh12	cadherin 12	-2.01	0.01	NM_001008420

Cdh19	cadherin 19, type 2	-3.52	0.04	NM_001081386
Cdh8	cadherin 8	-2.20	0.04	ENSMUST00000128860
Cdh9	cadherin 9	-2.18	0.03	NM_009869
Celsr2	cadherin, EGF LAG seven-pass G-type receptor 2 (flamingo homolog, Drosophila)	-2.65	0.03	NM_017392
Chga	chromogranin A	-2.95	0.01	NM_007693
Chl1	cell adhesion molecule with homology to L1CAM	-2.99	0.02	NM_007697
Chn1	chimerin (chimaerin) 1	-2.44	0.03	NM_001113246
Chrna4	cholinergic receptor, nicotinic, alpha polypeptide 4	-2.64	0.00	NM_015730
Cks2	CDC28 protein kinase regulatory subunit 2	2.07	0.03	NM_025415
Clstn2	calsyntenin 2	-2.86	0.03	NM_022319
Clstn3	calsyntenin 3	-2.83	0.03	NM_153508
Cnih3	cornichon homolog 3 (Drosophila)	-2.08	0.01	NM_028408
Cnksr2	connector enhancer of kinase suppressor of Ras 2	-5.63	0.01	NM_177751
Csmd3	CUB and Sushi multiple domains 3	-3.70	0.02	NM_001081391
Cyfip2	cytoplasmic FMR1 interacting protein 2	-2.79	0.02	NM_133769
D10Bwg1379e	DNA segment, Chr 10, Brigham & Women's Genetics 1379 expressed	-2.55	0.02	NM_001033258
D17H6S56E-5	DNA segment, Chr 17, human D6S56E 5	2.06	0.00	L78788
D430041D05Rik	RIKEN cDNA D430041D05 gene	-2.23	0.02	NM_001033347
Dbc1	deleted in bladder cancer 1 (human)	-2.51	0.04	NM_019967
Dbpht2	DNA binding protein with his-thr domain	-2.35	0.03	NM_198866
Dclk1	doublecortin-like kinase 1	-3.32	0.05	ENSMUST00000167204
Diras2	DIRAS family, GTP-binding RAS-like 2	-2.35	0.04	NM_001024474
Dnajc6	DnaJ (Hsp40) homolog, subfamily C, member 6	-2.82	0.04	NM_001164585
Dner	delta/notch-like EGF-related receptor	-3.28	0.04	NM_152915

Dock3	dedicator of cyto-kinesis 3	-3.78	0.03	NM_153413
Dpp10	dipeptidylpeptidase 10	-2.91	0.03	NM_199021
Dpp6	dipeptidylpeptidase 6	-2.74	0.02	NM_207282
Edil3	EGF-like repeats and discoidin I-like domains 3	-4.30	0.01	NM_001037987
Elmod1	ELMO domain containing 1	-3.82	0.02	NM_177769
Eno2	enolase 2, gamma neuronal	-3.19	0.04	NM_013509
Epha6	Eph receptor A6	-2.16	0.04	NM_007938
Faim2	Fas apoptotic inhibitory molecule 2	-5.57	0.01	NM_028224
Fam171b	family with sequence similarity 171, member B	-3.01	0.04	NM_175514
Fam19a1	family with sequence similarity 19, member A1	-2.14	0.03	NM_182808
Fam5c	family with sequence similarity 5, member C	-2.51	0.05	NM_153539
Fat3	FAT tumor suppressor homolog 3 (Drosophila)	-2.57	0.02	NM_001080814
Fbxl16	F-box and leucine-rich repeat protein 16	-2.62	0.04	NM_001164225
Fut9	fucosyltransferase 9	-5.22	0.01	NM_010243
Gabbr2	gamma-aminobutyric acid (GABA) B receptor, 2	-4.27	0.03	NM_001081141
Gabra1	gamma-aminobutyric acid (GABA) A receptor, subunit alpha 1	-9.38	0.01	NM_010250
Gabra3	gamma-aminobutyric acid (GABA) A receptor, subunit alpha 3	-3.34	0.03	NM_008067
Gabra5	gamma-aminobutyric acid (GABA) A receptor, subunit alpha 5	-3.38	0.04	NM_176942
Gabrb1	gamma-aminobutyric acid (GABA) A receptor, subunit beta 1	-3.88	0.03	ENSMUST00000031122
Gabrb2	gamma-aminobutyric acid (GABA) A receptor, subunit beta 2	-8.31	0.01	NM_008070
Gabrb3	gamma-aminobutyric acid (GABA) A receptor, subunit beta 3	-4.94	0.01	NM_008071
Gabrg2	gamma-aminobutyric acid (GABA) A receptor, subunit gamma 2	-9.06	0.01	ENSMUST00000070725
Gabrg3	gamma-aminobutyric acid (GABA) A	-3.52	0.02	NM_008074

receptor, subunit gamma 3

Gad2	glutamic acid decarboxylase 2	-2.84	0.02	NM_008078
Glrb	glycine receptor, beta subunit	-3.02	0.03	NM_010298
Gm10419	predicted gene 10419	-2.80	0.03	AK165889
Gm3893	predicted gene 3893	2.89	0.04	BC059060
Gm5567	predicted gene 5567	-5.05	0.02	NM_001004182
Gpr158	G protein-coupled receptor 158	-8.02	0.01	NM_001004761
Gpr165	G protein-coupled receptor 165	-2.18	0.05	NM_029536
Gpr22	G protein-coupled receptor 22	-2.15	0.01	NM_175191
Gpr37	G protein-coupled receptor 37	-4.05	0.04	ENSMUST00000054867
Gpr37l1	G protein-coupled receptor 37-like 1	-3.41	0.05	NM_134438
Gria1	glutamate receptor, ionotropic, AMPA1 (alpha 1)	-2.57	0.05	NM_001113325
Gria3	glutamate receptor, ionotropic, AMPA3 (alpha 3)	-4.95	0.05	NM_016886
Grik2	glutamate receptor, ionotropic, kainate 2 (beta 2)	-3.12	0.05	NM_010349
Grin2b	glutamate receptor, ionotropic, NMDA2B (epsilon 2)	-5.52	0.01	NM_008171
Grm1	glutamate receptor, metabotropic 1	-3.58	0.04	NM_016976
Grm3	glutamate receptor, metabotropic 3	-3.65	0.05	NM_181850
Grm5	glutamate receptor, metabotropic 5	-3.59	0.02	NM_001143834
Hcn1	hyperpolarization-activated, cyclic nucleotide-gated K+ 1	-4.80	0.01	NM_010408
Hmox1	heme oxygenase (decycling) 1	3.12	0.00	NM_010442
Igsf21	immunoglobin superfamily, member 21	-2.71	0.05	NM_198610
Itih3	inter-alpha trypsin inhibitor, heavy chain 3	-2.24	0.04	NM_008407
Kcna1	potassium voltage-gated channel, shaker-related subfamily, member 1	-3.70	0.03	NM_010595
Kcna2	potassium voltage-gated channel, shaker-related subfamily, member 2	-2.84	0.04	NM_008417
Kcna4	potassium voltage-gated channel,	-2.21	0.03	NM_021275

	shaker-related subfamily, member 4			
Kcnd2	potassium voltage-gated channel, Shal-related family, member 2	-4.56	0.03	NM_019697
Kcnh5	potassium voltage-gated channel, subfamily H (eag-related), member 5	-2.62	0.01	NM_172805
Kcnh7	potassium voltage-gated channel, subfamily H (eag-related), member 7	-3.04	0.03	NM_133207
Kcnip3	Kv channel interacting protein 3, calsenilin	-2.47	0.05	NM_019789
Kcnip4	Kv channel interacting protein 4	-2.02	0.04	NM_001199242
Kcnj3	potassium inwardly-rectifying channel, subfamily J, member 3	-2.97	0.04	ENSMUST00000067101
Kcnma1	potassium large conductance calcium-activated channel, subfamily M, alpha member 1	-2.72	0.02	NM_001253369
Kcnq3	potassium voltage-gated channel, subfamily Q, member 3	-2.15	0.01	NM_152923
Kcnq5	potassium voltage-gated channel, subfamily Q, member 5	-2.16	0.05	NM_001160139
Kcnv1	potassium channel, subfamily V, member 1	-2.99	0.04	NM_026200
Kif5c	kinesin family member 5C	-2.22	0.05	NM_008449
Kit	kit oncogene	3.91	0.00	NM_001122733
Lamb1	laminin B1	2.23	0.02	NM_008482
Lgi3	leucine-rich repeat LGI family, member 3	-4.12	0.03	NM_145219
Lmo3	LIM domain only 3	-2.59	0.02	NM_207222
Lonrf2	LON peptidase N-terminal domain and ring finger 2	-3.42	0.04	ENSMUST00000147695
Lphn1	latrophilin 1	-2.18	0.03	NM_181039
Lrg1	leucine-rich alpha-2-glycoprotein 1	2.23	0.04	NM_029796
Lrp1b	low density lipoprotein-related protein 1B (deleted in tumors)	-2.44	0.04	NM_053011
Lrrc4c	leucine rich repeat containing 4C	-4.04	0.02	NM_178725
Lrrn1	leucine rich repeat protein 1, neuronal	-4.15	0.04	NM_008516
Lrrtm2	leucine rich repeat transmembrane neuronal 2	-2.99	0.03	NM_178005

Lrrtm3	leucine rich repeat transmembrane neuronal 3	-3.89	0.02	NM_178678
Lrrtm4	leucine rich repeat transmembrane neuronal 4	-2.17	0.03	NR_027323
Mal2	mal, T cell differentiation protein 2	-3.73	0.03	NM_178920
Mapk10	mitogen-activated protein kinase 10	-3.36	0.02	NM_009158
Mapk8ip2	mitogen-activated protein kinase 8 interacting protein 2	-2.15	0.04	ENSMUST00000023291
Mdga2	MAM domain containing glycosylphosphatidylinositol anchor 2	-2.91	0.03	NM_001193266
Mgat4c	mannosyl (alpha-1,3-)-glycoprotein beta-1,4-N-acetylglucosaminyltransferase, isozyme C (putative)	-2.18	0.02	NM_001162369
Mtap2	microtubule-associated protein 2	-2.21	0.03	NM_001039934
Nalcn	sodium leak channel, non-selective	-2.02	0.02	NM_177393
Napb	N-ethylmaleimide sensitive fusion protein attachment protein beta	-2.58	0.02	ENSMUST00000028926
Ncam1	neural cell adhesion molecule 1	-3.53	0.02	NM_001081445
Ncam2	neural cell adhesion molecule 2	-3.93	0.03	NM_001113208
Ndst4	N-deacetylase/N-sulfotransferase (heparin glucosaminyl) 4	-2.63	0.01	NM_022565
Necab1	N-terminal EF-hand calcium binding protein 1	-3.82	0.01	NM_178617
Nell2	NEL-like 2 (chicken)	-4.15	0.03	NM_016743
Neto2	neuropilin (NRP) and tolloid (TLL)-like 2	-2.10	0.04	NM_001081324
Nkain2	Na+/K+ transporting ATPase interacting 2	-3.87	0.02	NM_001013411
Nlgn1	neuroligin 1	-2.96	0.05	NM_138666
Nlgn3	neuroligin 3	-3.08	0.02	NM_172932
Nos2	nitric oxide synthase 2, inducible	1.47	0.04	ENSMUST00000018610
Nova1	neuro-oncological ventral antigen 1	-4.15	0.04	NM_021361
Nox4	NADPH oxidase 4	1.90	0.01	ENSMUST00000032781
Nrcam	neuron-glia-CAM-related cell adhesion molecule	-3.10	0.01	NM_176930

Nrxn1	neurexin I	-3.87	0.03	NM_020252
Ntm	neurotrimin	-2.46	0.04	NM_172290
Ntrk3	neurotrophic tyrosine kinase, receptor, type 3	-2.21	0.05	ENSMUST00000039431
Nxph1	neurexophilin 1	-2.01	0.05	ENSMUST00000060369
Odz1	odd Oz/ten-m homolog 1 (Drosophila)	-2.51	0.02	NM_011855
Odz2	odd Oz/ten-m homolog 2 (Drosophila)	-2.07	0.04	NM_011856
Odz3	odd Oz/ten-m homolog 3 (Drosophila)	-3.40	0.02	NM_011857
Olfm1	olfactomedin 1	-2.00	0.02	NM_019498
Olfm3	olfactomedin 3	-2.39	0.04	NM_153157
Opcml	opioid binding protein/cell adhesion molecule-like	-4.39	0.02	NM_177906
Pak3	p21 protein (Cdc42/Rac)-activated kinase 3	-2.46	0.03	ENSMUST00000112863
Pcdh10	protocadherin 10	-3.69	0.04	NM_001098171
Pcdh9	protocadherin 9	-4.53	0.02	NM_001081377
Pclo	piccolo (presynaptic cytomatrix protein)	-2.41	0.02	NM_001110796
Pdlim1	PDZ and LIM domain 1 (elfin)	4.07	0.01	NM_016861
Pgf	placental growth factor	4.11	0.00	NM_008827
Pnmal2	PNMA-like 2	-2.08	0.05	NM_001099636
Prg4	proteoglycan 4 (megakaryocyte stimulating factor, articular superficial zone protein)	2.38	0.00	NM_021400
Prkca	protein kinase C, alpha	-2.09	0.05	NM_011101
Prkcg	protein kinase C, gamma	-2.55	0.04	NM_011102
Prnd	prion protein dublet	5.95	0.01	NM_023043
Ptk2b	PTK2 protein tyrosine kinase 2 beta	-2.18	0.04	NM_001162365
Ptprn	protein tyrosine phosphatase, receptor type, N	-2.54	0.04	NM_008985
Ptprn2	protein tyrosine phosphatase, receptor type, N polypeptide 2	-2.07	0.04	NM_011215
Ptprt	protein tyrosine phosphatase, receptor type, T	-2.23	0.05	NM_021464

Ptprz1	protein tyrosine phosphatase, receptor type Z, polypeptide 1	-3.91	0.05	NM_001081306
Pxdn	peroxidasin homolog (Drosophila)	3.24	0.00	NM_181395
Raet1d // Raet1b // Raet1a	retinoic acid early transcript delta // retinoic acid early transcript beta // retinoic acid early transcript 1, alpha	2.60	0.01	ENSMUST00000130977
Raet1e // Raet1c	retinoic acid early transcript 1E // retinoic acid early transcript gamma	2.29	0.02	ENSMUST00000065527
Rasgrp1	RAS guanyl releasing protein 1	-6.40	0.01	NM_011246
Reln	reelin	-3.65	0.00	NM_011261
Robo2	roundabout homolog 2 (Drosophila)	-2.53	0.01	NM_175549
Rtn1	reticulon 1	-4.01	0.02	NM_153457
Scn1a	sodium channel, voltage-gated, type I, alpha	-2.06	0.00	NM_018733
Scn2a1	sodium channel, voltage-gated, type II, alpha 1	-8.76	0.01	NM_001099298
Sele	selectin, endothelial cell	2.19	0.01	NM_011345
Selp	selectin, platelet	5.70	0.01	NM_011347
Serpine1	serine (or cysteine) peptidase inhibitor, clade E, member 1	5.44	0.00	NM_008871
Sez6l2	seizure related 6 homolog like 2	-4.26	0.03	NM_144926
Sfrp4	secreted frizzled-related protein 4	2.85	0.01	ENSMUST00000169327
Slc17a7	solute carrier family 17 (sodium-dependent inorganic phosphate cotransporter), member 7	-6.75	0.02	NM_182993
Slc24a2	solute carrier family 24 (sodium/potassium/calcium exchanger), member 2	-5.78	0.01	NM_172426
Slc2a13	solute carrier family 2 (facilitated glucose transporter), member 13	-2.82	0.01	NM_001033633
Slc6a1	solute carrier family 6 (neurotransmitter transporter, GABA), member 1	-4.18	0.04	NM_178703
Slc6a11	solute carrier family 6 (neurotransmitter transporter, GABA), member 11	-5.60	0.01	NM_172890
Slc6a9	solute carrier family 6 (neurotransmitter transporter, glycine), member 9	-2.42	0.04	ENSMUST00000063857

Slc7a14	solute carrier family 7 (cationic amino acid transporter, y+ system), member 14	-4.34	0.00	NM_172861
Slc8a1	solute carrier family 8 (sodium/calcium exchanger), member 1	-5.23	0.00	NM_011406
Slco2a1	solute carrier organic anion transporter family, member 2a1	2.40	0.03	NM_033314
Slitrk1	SLIT and NTRK-like family, member 1	-2.32	0.05	NM_199065
Slitrk3	SLIT and NTRK-like family, member 3	-3.95	0.03	NM_198864
Slitrk4	SLIT and NTRK-like family, member 4	-2.09	0.01	NM_178740
Snap25	synaptosomal-associated protein 25	-4.33	0.02	NM_011428
Snora31	small nucleolar RNA, H/ACA box 31	3.74	0.04	NR_028481
Snora33	small nucleolar RNA, H/ACA box 33	6.13	0.04	NR_037680
Snora44	small nucleolar RNA, H/ACA box 44	2.09	0.02	NR_034050
Snora73b	small nucleolar RNA, H/ACA box 73b	2.12	0.04	NR_028513
Sorcs1	VPS10 domain receptor protein SORCS 1	-2.01	0.03	NM_021377
Sorcs3	sortilin-related VPS10 domain containing receptor 3	-2.54	0.03	NM_025696
Sorl1	sortilin-related receptor, LDLR class A repeats-containing	-2.88	0.03	NM_011436
Sphkap	SPHK1 interactor, AKAP domain containing	-2.87	0.01	ENSMUST00000160953
Spock1	sparc/osteonectin, cwcv and kazal-like domains proteoglycan 1	-2.66	0.03	NM_009262
Spon1	spondin 1, (f-spondin) extracellular matrix protein	-2.41	0.03	NM_145584
Sprn	shadow of prion protein	-2.14	0.05	NM_183147
Srgap3	SLIT-ROBO Rho GTPase activating protein 3	-2.38	0.05	NM_080448
Sstr2	somatostatin receptor 2	-2.04	0.03	NM_009217
St6gal2	beta galactoside alpha 2,6 sialyltransferase 2	-4.81	0.01	NM_172829
St8sia5	ST8 alpha-N-acetyl-neuraminide alpha-2,8-sialyltransferase 5	-3.69	0.01	NM_013666
Stxbp5l	syntaxin binding protein 5-like	-3.68	0.03	NM_172440

Sv2a	synaptic vesicle glycoprotein 2 a	-3.60	0.04	NM_022030
Sv2b	synaptic vesicle glycoprotein 2 b	-11.75	0.00	NM_001109753
Syn1	synapsin I	-3.14	0.03	NM_013680
Syn2	synapsin II	-2.32	0.03	NM_001111015
Syngr3	synaptogyrin 3	-2.21	0.04	NM_011522
Syp	synaptophysin	-3.29	0.04	NM_009305
Syt1	synaptotagmin I	-9.31	0.02	NM_001252341
Syt5	synaptotagmin V	-3.15	0.02	NM_016908
Tbr1	T-box brain gene 1	-3.06	0.02	NM_009322
Thbs1	thrombospondin 1	2.02	0.00	NM_011580
Timp1	tissue inhibitor of metalloproteinase 1	2.51	0.00	NM_001044384
Tmem130	transmembrane protein 130	-4.09	0.01	NM_177735
Tmem56	transmembrane protein 56	-2.62	0.02	ENSMUST00000029777
Tmem59l	transmembrane protein 59-like	-2.35	0.02	NM_182991
Tnfrsf23	tumor necrosis factor receptor superfamily, member 23	2.12	0.02	NM_024290
Tnr	tenascin R	-4.80	0.03	NM_022312
Trim2	tripartite motif-containing 2	-2.20	0.05	ENSMUST00000107691
Trp53i11	transformation related protein 53 inducible protein 11	2.21	0.00	NM_001025246
Tubb6	tubulin, beta 6 class V	2.80	0.00	NM_026473
Ube2ql1	ubiquitin-conjugating enzyme E2Q family-like 1	-3.38	0.04	NM_001145162
Unc5a	unc-5 homolog A (C. elegans)	-2.31	0.04	ENSMUST00000026994
Upp1	uridine phosphorylase 1	2.77	0.02	NM_009477
Vsig4	V-set and immunoglobulin domain containing 4	2.43	0.00	NM_177789
Vsnl1	visinin-like 1	-5.67	0.01	NM_012038
Vstm2a	V-set and transmembrane domain containing 2A	-3.20	0.02	NM_145967
Xylt1	xylosyltransferase 1	-2.15	0.05	NM_175645

Supplemental Figure
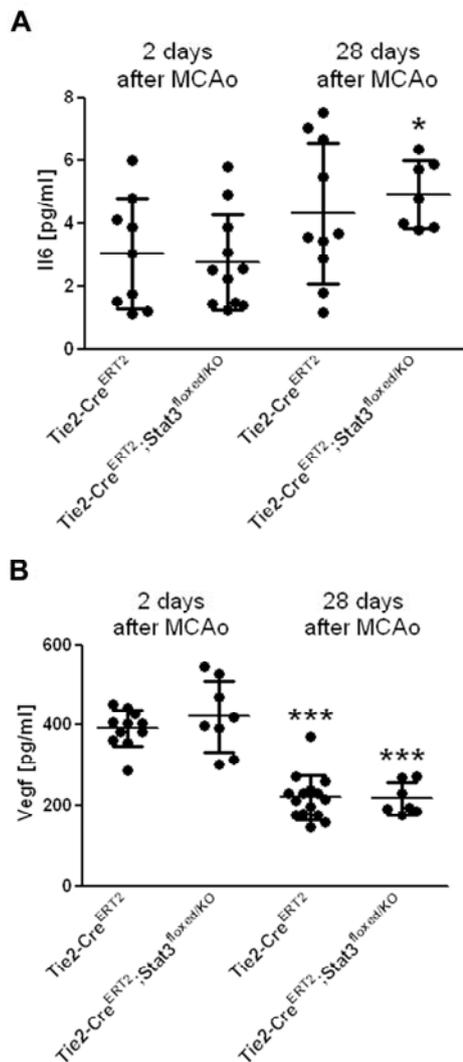
Supplemental Figure 1. Endothelial Stat3 has no impact on systemic Il6 and Vegf serum levels after cerebral ischemia. Serum levels of Il6 **(A)** were determined at 2 days and 28 days after cerebral ischemia. Data are presented as scatter dot blots with mean ± s.d. Two way ANOVA was followed by Tukey's posthoc analysis with $F_{(1,36)}$ = 8.6 for reperfusion time point with p = 0.006. There was no significant difference between genotypes with $F_{(1,36)}$ = 0.08 and p = 0.78. *p = 0.02 versus corresponding 2 days reperfusion time points within the same genotype group. Serum levels of Vegf **(B)** were determined 2 days and 28 days after cerebral ischemia. Data are presented as scatter dot blots with mean ± s.d. Two way ANOVA was followed by Tukey's posthoc analysis with $F_{(1,40)}$ = 94.4 for reperfusion time point with p < 0.001. There was no significant difference between genotypes with $F_{(1,40)}$ = 0.5 and p = 0.51. ***p < 0.001 versus corresponding 2 days reperfusion time points within the same genotype group.

Supplemental References

1.   Takeda K, Kaisho T, Yoshida N, Takeda J, Kishimoto T and Akira S. Stat3 activation is responsible for IL-6-dependent T cell proliferation through preventing apoptosis: generation and characterization of T cell-specific Stat3-deficient mice. *J Immunol*. 1998;161:4652-60.
2.   Forde A, Constien R, Grone HJ, Hammerling G and Arnold B. Temporal Cre-mediated recombination exclusively in endothelial cells using Tie2 regulatory elements. *Genesis*. 2002;33:191-7.
3.   Endres M, Gertz K, Lindauer U, Katchanov J, Schultze J, Schrock H, Nickenig G, Kuschinsky W, Dirnagl U and Laufs U. Mechanisms of stroke protection by physical activity. *Ann Neurol*. 2003;54:582-90.
4.   Bederson JB, Pitts LH, Tsuji M, Nishimura MC, Davis RL and Bartkowski H. Rat middle cerebral artery occlusion: evaluation of the model and development of a neurologic examination. *Stroke; a journal of cerebral circulation*. 1986;17:472-6.
5.   Olah M, Amor S, Brouwer N, Vinet J, Eggen B, Biber K and Boddeke HW. Identification of a microglia phenotype supportive of remyelination. *Glia*. 60:306-21.
6.   Irizarry RA, Hobbs B, Collin F, Beazer-Barclay YD, Antonellis KJ, Scherf U and Speed TP. Exploration, normalization, and summaries of high density oligonucleotide array probe level data. *Biostatistics*. 2003;4:249-64.

Supplemental video legend

Supplemental movie 1. Post-ischemic angiogenesis is reduced after endothelial-specific ablation of Stat3. Tie2-Cre^{ERT2} littermates (n=11) and Tie2-Cre^{ERT2};Stat3$^{floxed/KO}$ (n=7) were subjected to 30 min MCAo after 5 days of daily tamoxifen administration followed by a free interval of 2 days and were killed 28 days after cerebral ischemia and stained for caveolin-1. Confocal images of isolectin B4 stained vascular networks were collected with a spinning disc system consisting of a Axio Observer Z.1 microscope (Zeiss, Jena, Germany) equipped with a Yokogawa CSU-X1 unit using a 20x/0.4 Korr M27 objective and processed with ZEN2012 software (Zeiss, Jena, Germany). Orthogonal projections (60 µm) and supplementary movie were generated by ImageJ. 3D projections of peri-infarct vascular networks.